Design and development of novel titanium alloys with enhanced wear resistance for biomedical implant applications

By

Lisseth Katherine Ramírez Antolínez

Thesis
Submitted to Flinders University
for the degree of

Master of Engineering (Mechanical)

College of Science and Engineering

June 2024

TABLE OF CONTENTS

ABSTRACT

The field of biomaterials has seen significant growth, becoming a burgeoning industry and a key area of research. The widespread adoption of titanium and its alloys in biomedical applications, particularly in devices with metal-to-metal contacting parts, has been fueled by their exceptional attributes: low density, high specific strength, favorable mechanical properties, high biocompatibility, and excellent corrosion resistance. This expansion is largely driven by the demand for durable implants and prostheses that can effectively serve an aging population. Previous research has demonstrated that alloying titanium with elements like Zr, Nb, Ta, and Mo can significantly enhance its mechanical properties and biocompatibility. In this project, a series of Ti-xZr-4Nb-33Ta (x=20, 30, 40 wt.%) and Ti-30Zr-4Nb-xMo (x=10, 13, 16 wt.%) alloys were specifically designed and fabricated via casting techniques. The microstructural characteristics, mechanical properties, and wear resistance in Phosphate-Buffered Saline solution were comprehensively assessed for all six alloys, with comparisons made against the widely used Ti-6Al-4V alloy. Optical microscopy of the Ti-Zr-Nb-Ta, Ti-6Al-4V, and Ti-Zr-Nb-Mo alloys revealed homogeneous grain structures with visible pores and surface contaminants. Nanoindentation tests showed that the nanohardness values of the tested alloys ranged from 3.9 to 5.3 GPa. Among the Ta-containing alloys, Ti-20Zr-4Nb-33Ta (H = 4.5 ± 0.07 GPa) and Ti-40Zr-4Nb-33Ta (H = 4.4 ± 0.09 GPa) exhibited similar hardness values, while Ti-30Zr-4Nb-33Ta showed slightly lower hardness (H = 4.2 ± 0.17 GPa). In the Mo-containing alloys, an increase in Mo content generally correlated with an increase in nanohardness, with Ti-30Zr-4Nb-16Mo demonstrating the highest hardness (H = 5.3 ± 0.24 GPa). Young's modulus for the Ti-Zr-Nb-Ta and Ti-Zr-Nb-Mo alloys ranged from 70 to 108 GPa, all lower than the Ti-6Al-4V reference value of 120 GPa. Tribocorrosion tests at open circuit potential (OCP) showed that both Ta- and Mo-containing alloys exhibited superior wear resistance compared to Ti-6Al-4V, specifically the Ti-30Zr-4Nb-16Mo alloy demonstrated the lowest wear potentials under varying normal loads (17.5 N and 30.8 N), indicating enhanced tribocorrosion resistance. Scanning electron microscopy (SEM) of the wear tracks revealed significant differences in wear mechanisms and track morphology under different load conditions, with higher loads resulting in increased abrasive wear and plastic deformation.

The results suggest that the novel Ti-Zr-Nb-Ta and Ti-Zr-Nb-Mo developed alloys possess promising mechanical and tribocorrosion properties, making them suitable candidates for biomedical implant applications. The improved wear resistance and lower Young's modulus compared to Ti-6Al-4V indicate their potential to reduce the stress-shielding effect and enhance implant longevity. This study fills the gap in understanding the comprehensive properties of these novel alloys, providing a foundation for their future application in biomedical devices.

DECLARATION

I certify that this thesis:

1. does not incorporate without acknowledgment any material previously submitted for a degree or diploma in any university
2. and the research within will not be submitted for any other future degree or diploma without the permission of Flinders University; and
3. to the best of my knowledge and belief, does not contain any material previously published or written by another person except where due reference is made in the text.

Signature of student

Print name of student   **Lisseth Katherine Ramírez Antolínez**

Date   **06.06.2024**

I certify that I have read this thesis. In my opinion **it is**/~~is not~~ fully adequate, in scope and in quality, as a thesis for the degree of Master of Engineering (Mechanical). Furthermore, I confirm that I have provided feedback on this thesis and the student has implemented it ~~minimally/partially/~~**fully**.

Signature of Principal Supervisor.....

Print name of Principal Supervisor **Reza Hashemi**

Date   **06.06.2024**

ACKNOWLEDGEMENTS

LIST OF FIGURES

LIST OF TABLES

PUBLICATIONS FROM THESIS

The findings from this thesis have been included in a manuscript which is currently being reviewed by my supervisor for a journal article submission with the following details:

Ramirez Antolinez LK., Feyzi M., Xiao W., Hashemi R. Design and development of novel titanium alloys with enhanced wear resistance for biomedical implant applications. Article to be submitted to Biomaterials Advances (Formerly known as Materials Science and Engineering: C)

1   INTRODUCTION

Metals had been crucial in orthopedic surgery and orthodontic practices[1], despite a wide range of metals and alloys, only few are suitable due to biocompatibility and long-term effectiveness. Biomedical metals can be categorized into stainless steels, cobalt-based alloys, titanium-based alloys, and magnesium-based alloys. Since the 1950s, commercially pure titanium and its alloys have consistently held a prominent position in biomedical applications due to their remarkable combination of mechanical strength, corrosion resistance, biocompatibility, and inherent antibacterial properties[2]. These attributes make titanium an ideal biomaterial for implants. Notably, titanium facilitates osseointegration, a crucial process where the implant bonds naturally with living bone without the need for additional adhesives [2]. Titanium and its alloys are utilized in implant devices that replace compromised hard tissues, including artificial hip and knee joints, bone plates, and dental implants. Additionally, titanium and its alloys are used in dental products like crowns, bridges, and dentures, which are typically produced using precision casting techniques[3]. Titanium-based alloys are categorized into four groups: α, near-α, α–β, and β alloys. The α–β alloy Ti–6Al–4V is the most widely used, accounting for approximately 45% of all titanium production. The key elements for medical implants include V, Al, Nb, Zr, Mo, Fe, and Ta [1]. Alloying elements are divided into three categories based on the phases they stabilize. These stabilizers can alter the temperatures at which certain phases remain stable: α stabilizers (O, Al, N, C) increase the temperature at which the α phase is stable, while β stabilizers (such as V, Nb, Mo, and Ta) decrease the temperature at which the β phase is stable. Ti-6Al-4V is a prominent titanium alloy for biomedical applications due to its excellent corrosion resistance, dual-phase α + β microstructure that provides a high elastic modulus, and recognized biocompatibility [4]. However, there are concerns about the release of aluminium and vanadium ions from Ti-6Al-4V, which could pose health risks such as Alzheimer's disease and neuropathy [1]. A key characteristic of a titanium alloy implant is that its mechanical properties must closely match those of human bones to ensure effective functionality. The discrepancy between bone's Young's modulus (10-30 GPa) [5] and those of Ti alloys (ranging from 100 to 110 GPa) [6] leads to stress shielding between the implant and the surrounding bone tissue. Normally, bone bears the entire load, but with an implant, stress is shared. This triggers bone adaptation, causing increased mass in heavily loaded areas and bone resorption in lighter areas, risking implant failure[5]. Other Challenge that titanium-based alloys face is due to friction, generating metal debris [7] , often seen in post-mortem studies of patients with total hip or knee replacements [8]. Their high friction

coefficient and low surface hardness lead to limited wear resistance, causing implant loosening, especially in total joint replacements (TJR) [5]. TJR procedures, using metallic femoral heads and polymer acetabular cups, experience higher wear rates than Co-Cr-Mo alloys [5]. This is mainly due to the mechanical instability of the oxide film on titanium alloy surfaces, hindering passivation reestablishment and posing a significant challenge in TJR application. This issue is presented in Figure 1.
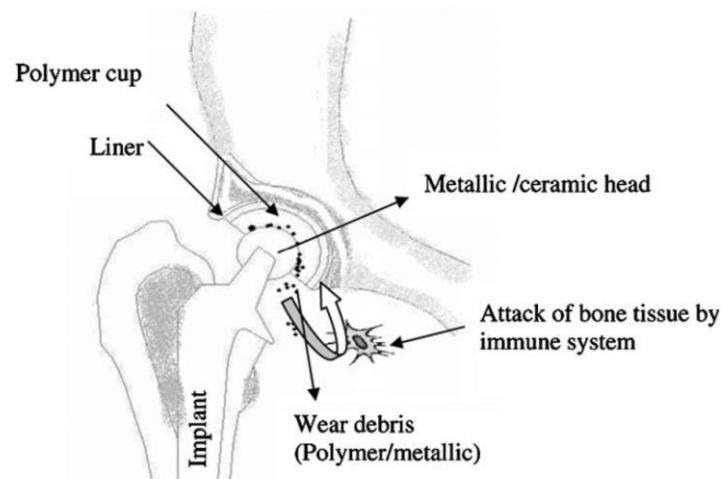
Figure 1. Mechanism of hip implant failure, attributed to wear particle release inducing bone resorption, leading to implant loosening[1] [8]

To address these challenges, researchers have explored the development of novel titanium alloys with enhanced properties. This thesis focuses on the design, fabrication, and comprehensive evaluation of a series of Ti-xZr-4Nb-33Ta (x=20, 30, 40 wt.%) and Ti-30Zr-4Nb-xMo (x=10, 13, 16 wt.%) alloys. The study assesses the microstructural characteristics, mechanical properties, and wear resistance of these novel alloys in a Phosphate-Buffered Saline (PBS) solution, comparing them with the widely used Ti-6Al-4V alloy. The research aims to fill the gap in understanding the comprehensive properties of these novel alloys, providing a foundation for their future application in biomedical devices.

2 CHAPTER ONE: LITERATURE REVIEW

2.1 Low-stiffness titanium alloys to minimize stress shielding

Second-generation titanium biomaterials, like titanium alloys, aim to address stress shielding by matching the modulus of bone more closely. Developed predominantly in the 1990s, these alloys offer lower elastic module, superior corrosion resistance, and enhanced biocompatibility compared to Ti–6Al–4V and other α-β alloys[1]. They are composed of

---

[1] Reprinted with permission from Elsevier

biocompatible elements like niobium, zirconium, molybdenum, tantalum, and iron, omitting vanadium. Notably, the Ti–Nb–Zr–Ta system (TNZT alloys) boasts the lowest elastic module among metallic implant alloys developed to date[9]. The new generation β-type Titanium alloys with non-toxic element systems have been developed recently [10] are presented in Appendice 1. The microstructure and mechanical properties of a series of high zirconium alloys, specifically Ti–30Zr–xMo alloys, were evaluated in [11]. The investigation focused on how varying Mo content influenced both properties. Alloys with 5Mo, 6Mo, 7Mo, and 8Mo (wt%) showed lower Young's modulus, ranging from 90 GPa (with 2Mo) to around 60 GPa (with 6Mo), compared to Ti-6Al-4V. However, wear resistance was not assessed in this study.The results are presented in Figure 2. Recent research examined the microstructure and mechanical properties of new Titanium alloys, such as Ti-23Nb-7Zr, Ti-28Nb-7Zr, and Ti-33Nb-7Zr (wt%). The addition of niobium stabilized the β phase while reducing α´ and α″ phases. These alloys show potential for orthopedic implants pending further biocompatibility testing [12]. New developed titanium alloys with Mo, Si, Zr, and Ta, offering reduced modulus, increased corrosion resistance, and improved biocompatibility were assessed with Ti-15Mo-0.5Si showed the lowest young modulus at 19.81 GPa [13]. In biomedical contexts, materials that are compatible with cellular activity, known as cytocompatible materials, are essential for the successful integration of implants, devices, and medical interventions by fostering favorable cell behavior within the body. To assess their suitability for orthopedic applications, newly developed beta (β)-type Ti-Nb-Zr-Mo (TNZM) alloys underwent mechanical testing and cytocompatibility evaluations. These alloys, including Ti-24Nb-38Zr-2Mo, Ti-27Nb-33Zr-2Mo, Ti-30Nb-28Zr-2Mo, and Ti-37Nb-16Zr-2Mo, exhibited a body-centered-cubic structure (β-type) as their primary phase, with Ti-27Nb-33Zr-2Mo displaying the highest Vickers hardness (244 ±8 HV) and a Young's modulus ranging from 68 to 73 GPa. Assessment of cytocompatibility revealed that all TNZM alloys demonstrated favorable compatibility with cellular components.[14]
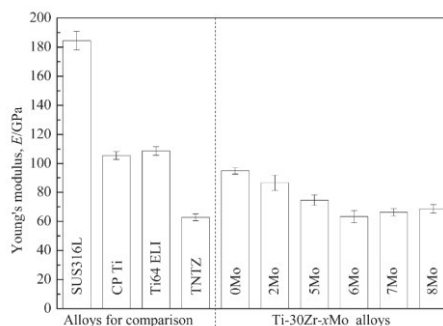

Figure 2. Young's modulus of Ti-30Zr-X Mo alloys[2][11]

2 Reprinted with permission from Elsevier

2.2 Improving wear resistance of Ti alloys

There is a necessity to improve the wear resistance of titanium alloys employed in biomedical applications. The wear mechanisms of these alloys can generally be classified into abrasive wear and adhesive wear. Compared to other biomaterials such as Co–Cr alloys and alumina, titanium alloys generally show lower wear resistance. The wear loss of biomedical titanium alloys is reduced in a simulated body fluid compared to in air [15], adhesive wear is the predominant wear mechanism within a living body. To overcome these challenges, researchers have explored various strategies to enhance the wear resistance of titanium alloys. Studies have investigated the wear and electrochemical corrosion behavior of specific titanium alloys such as Ti-5Al-2.5Fe and Ti-6Al-4V in simulated body fluid environments. Hardness values were determined as 706.6 HV for Ti-5Al-2.5Fe and 630 HV for Ti-6Al-4V, with structural analysis revealing dominance of the α-Ti phase. Ti-5Al-2.5Fe exhibited superior wear resistance attributed to its higher hardness, which effectively resisted wear, particularly under lower loads (10 N, 20 N), while maintaining alloy integrity [16]. In clinical dental practice, significant wear of titanium teeth has been noted following the use of cast titanium prostheses. The wear behavior of teeth made from various cast titanium alloys containing copper was examined and compared to commercially pure (CP) titanium, Ti–6Al–4V, and gold alloy [17]. Wear testing involved repeatedly grinding upper and lower teeth under flowing water using an experimental testing apparatus. Wear resistance was measured as volume loss (mm³) at a grinding force of 5 kgf after 50,000 strokes. The six types of titanium exhibited greater wear compared to the gold alloy. The experimental CP Ti+Cu and Ti–6Al–4V+Cu alloys showed superior wear resistance compared to CP titanium and Ti–6Al–4V, respectively. Although the gold alloy had the best wear properties, the 4% Cu in the Ti–6Al–4V alloy demonstrated the most favorable results among the titanium alloys. The addition of copper, forming the Ti/Ti2Cu eutectoid, appeared to enhance wear resistance. Ti–6Al–4V and Ti–24Al–11Nb alloys were also assessed for dry sliding wear conditions against hardened-steel counterparts in [18].Ti–24Al–11Nb displayed significantly superior wear resistance (approximately 48 times) compared to Ti–6Al–4V under a 45 N load. Ti–6Al–4V exhibited lower wear resistance due to severe delamination, whereas Ti–24Al–11Nb showed delamination with lower severity and oxidative wear. The formation of a protective oxide layer during wear contributed to Ti–24Al–11Nb's reduced wear rate. There is limited data on the wear resistance of dental alloys, particularly titanium alloys. Alloys of Ti–5Zr, Ti–5Ta, and Ti–5Ta–5Zr (%wt) were evaluated, revealing enhanced wear resistance with the addition of tantalum and zirconium. Zirconium also increased the microhardness of the Ti–5Zr alloy[19].
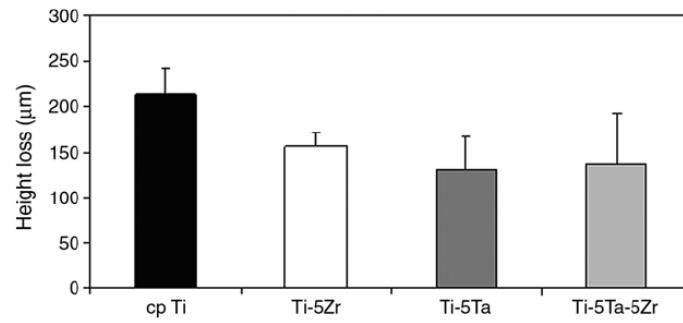
Figure 3. Height loss of cp Ti, Ti–5Zr, Ti–5Ta, Ti-5Ta-5Zr alloys[3] [19]

[20] studied Ti–30Zr, Ti–20Zr– 10Nb and Ti–19Zr–10Nb–1Fe. The addition of Nb showed the increase wear resistance of NiTi alloys. The Ti–20Zr–10Nb alloy exhibits superior wear resistance compared to the Ti–19Zr–10Nb–1Fe alloy due to the tendency of iron oxide to dislodge easily, resulting in fewer Nb_2O_5 films forming on the worn surface of the latter. The microstructure, electrochemical properties, and wear performance of various titanium-copper biomedical alloys (Ti-xCu, where x = 3, 7.1, and 12%wt) produced through powder metallurgy for dental implant applications were evaluated[21]. When tested in artificial saliva, these alloys showed increased eutectoid content at the grain boundary and facilitated the formation of Ti2Cu intermetallic compounds, which enhanced their hardness. The inclusion of copper also intensified the cathodic reaction and slightly increased the anodic reaction rate. As a result, a higher content of Ti2Cu intermetallic compounds led to decreased material loss due to wear and corrosion.

2.3 Gaps in the literature and aims

The research of titanium alloys displays a significant division. While one stream concentrates on reducing the Young's modulus, often overlooking wear resistance, another focuses solely on enhancing wear resistance without comparing new alloys to the industry-standard Ti-6Al-4V. Moreover, some studies compromise biocompatibility by introducing non-biocompatible elements. The fundamental question of whether new titanium alloys can simultaneously improve wear resistance, reduce Young's modulus, and maintain biocompatibility remains unanswered. Bridging this gap is imperative for advancing biomedical applications in the field.

---

[3] Reprinted with permission from Elsevier

3 CHAPTER TWO: METODOLOGY

3.1 Material characterization

3.1.1 Design of Titanium-based alloys

The chemical composition of the newly developed titanium alloys, aimed at enhancing wear resistance in biomedical applications, was meticulously formulated based on an extensive literature review, detailed in Appendice 2, Appendice 3, Appendice 4 Titanium alloys exist in three phases: α, α + β, and β, depending on their composition and formation temperature[4]. Research examining the impact of alloying elements on the strength and modulus of β-type biomedical titanium alloys indicates that non-toxic and non-allergenic elements such as Nb, Mo, Zr, and Ta encourage the development of β-type Ti alloys with increased strength and decreased Young's modulus [22]. Of these elements, Nb is regarded as the most biocompatible β-stabilizing element [23]. Several studies have indicated that higher levels of Nb result in a reduction in wear resistance [24], [25], [26], [27], [28]. Therefore, the wt% of Nb was fixed at 4 wt% in the six alloys proposed for this study. Ti–Nb–Zr–Ta alloys stand out for their low E value, promising mechanical properties, and excellent cytocompatibility[29], [30]. [31] introduced three new beta titanium alloys: Ti-38.3Ta-22Zr-8.1Nb (wt%), Ti-38.9Ta-25Zr-5Nb (wt%), and Ti-39.5Ta-28Zr-2.5Nb (wt%), exhibiting Young's module of 73.12±4.43 GPa, 74.98±2.19 GPa, and 76.62±2.38 GPa, respectively. The corresponding micro-hardness values were measured at 364.6±3.3 HV, 422.5±9.6 HV, and 433.4±7.9 HV, respectively. As per Achard's law[32], a direct correlation exists between the material's wear resistance and hardness. Consequently, elevating the material's hardness can enhance its capacity to withstand compressive deformation, improving its resistance to wear. Isomorphous stabilizers like Mo, Nb, and Ta have the potential to improve both strength and plasticity[33].High entropy alloys (HEAs) demonstrate favorable characteristics including high strength, hardness, and excellent resistance to wear, making them a focal point of research interest[34]. Molybdenum (Mo) is a non-toxic and hypoallergenic element frequently utilized in alloying due to its robust corrosion resistance. [35] investigated the microhardness values of Ti-15Mo-6Zr (wt%) and a range of Ti-15Mo-6Zr-xCr (wt%) alloys, finding consistent values between 368 and 412 HV. Six novel titanium alloys were formulated for this study. The compositions, given in weight percent (wt%), include Ti-40Zr-4Nb-33Ta, Ti-30Zr-4Nb-33Ta, Ti-20Zr-4Nb-33Ta, Ti-30Zr-4Nb-10Mo, Ti-30Zr-4Nb-13Mo, and Ti-30Zr-4Nb-16Mo.

3.1.2 Material preparation

Ti-Zr-Nb-Ta and Ti-Zr-Nb-Mo alloys were prepared by an arc-melting technique using high-purity Ti, Zr, Nb, Ta, Mo (99.9%). The ingots underwent five times remelting to ensure the homogeneity. After machining, cube-shaped samples measuring 10 mm x 10 mm x 10 mm were fabricated using a precision saw. These samples underwent hot compression mounting with phenolic resin (Multi-Fast) initially. Subsequently, the surface preparation involved a three-step automatic method. Plane grinding was performed using a rigid disk MD-Mezzo 220 with resin-bonded diamonds, followed by fine grinding using disk MD-largo with a 9 μm diamond suspension. Finally, chemical-mechanical polishing was conducted with disk MD-Chem, utilizing a mixture of colloidal silica (OP-S) and hydrogen peroxide (concentration between 10-30%). This process resulted in a mirror-like appearance of the samples. For more detailed information, please refer to Appendice 5.

To conduct the wear test, the samples underwent sequential grinding using 120, 240, 400, 600, and 1200 grit sandpapers. Teflon tape was meticulously applied to the lateral face of each sample. Subsequently, the samples were carefully positioned within 3D printing inserts and sealed with silicone adhesive, allowing for a 24-hour drying period. Additional Teflon tape was then added to the lateral face of the insert before placing it inside the chamber. Finally, the exposed surfaces of the samples were cleaned using methanol.

3.2 Surface and microstructural analysis

3.2.1 Optical Microscopy

The metallographic microstructure of Ti-Zr-Nb-Ta,Ti-Zr-Nb-Mo and Ti-6Al-4V alloys was examined by optical microscopy ZEISS Axio Imager M2M at Flinders University (Adelaide, SA, Australia) under 5x magnification, 10 x magnification, 20x magnification and 50x magnification.

3.2.2 Scanning Electron Microscopy (SEM), Energy Dispersive X-ray Spectroscopy (EDS)

The microstructure observation and compositional analyses of Ti-Zr-Nb-Ta,Ti-Zr-Nb-Mo and Ti-6Al-4V alloys were conducted using a FEI Inspect F50 Field Emission SEM (Flinders University, Adelaide, SA, Australia). SEM images were captured in backscattered electron (BSE) mode with an accelerating voltage of 30 kV, a spot size of 5.0, and a working distance of approximately 10 mm.

3.3 Mechanical Testing

3.3.1 Nanoindentation

The modulus of elasticity (E) and nano-hardness (H) of the titanium alloys were determined using load-displacement curves from nano-indentation tests, analyzed according to the Oliver and Pharr method [36]. These tests were conducted using an IBIS Nanoindentation System with a Berkovich diamond indenter at the University of Adelaide (Adelaide, SA, Australia), applying a maximum load of 100 mN. Each sample underwent at least 16 indentations, with the results averaged. To prevent the influence of residual strain between adjacent indentations, the indentations were spaced 25 μm apart. The equations for Oliver and Pharr method can be found in Appendice 12.

3.3.2 Microhardness

The Vickers hardness of the as-cast Ti-Zr-Nb-Ta, Ti-Zr-Nb-Mo and Ti-6Al-4V alloys was tested using a Struers DuraScan-20 microhardness tester fitted with a diamond indenter at Flinders University (Adelaide, SA, Australia). The measurements were taken under a load of 5 HV (49.03 N) and a dwell time of 3 s. Eight readings were taken at different positions on each alloy and the average and standard deviation was calculated.

3.4 Tribocorrosion test at OCP

The reciprocating wear behavior of the titanium alloys was evaluated using a custom ball-on-disk tribotester. Zirconia balls ZrO_2 (≥ 96%), with a diameter of 9.525 mm were used as the mating material. Three levels of normal forces were applied: 6 N, 17.5 N, and 30.8 N, corresponding to maximum initial Hertzian contact pressures of 704.8 MPa, 1007 MPa, and 1215.9 MPa, respectively. The sliding frequency was set to 3 Hz, with a sliding amplitude of 3 mm, and each test consisted of 5000 cycles. All tests were conducted in a phosphate buffer solution (PBS). The tribotester was equipped with a three-electrode setup. In the experiment, the working electrode comprised the titanium alloy samples with an exposed surface area of 100 mm^2, while a platinum plate served as the counter electrode. The reference electrode used was Ag/AgCl. The equipment was connected to a potentiostat (MetrOhm; Model: PGSTAT 204, Switzerland), enabling the application of a constant cathodic/anodic potential to the interface and recording of tribocorrosion current data.

4 CHAPTER THREE: RESULTS

4.1 Surface and microstructural analysis

4.1.1 Optical Microscopy

Figure 4,Figure 5,Figure 6 presents the metallographic images of the Ti-Zr-Nb-Ta, Ti-6Al-4V and Ti-Zr-Nb-Mo and alloys respectively. The optical micrographs for the Ti-Zr-Nb-Ta and Ti-Zr-Nb-Mo alloys did not reveal distinct grain structures, indicating potential challenges in distinguishing microstructural features at the magnifications used. Similarly, the microstructure of the Ti-6Al-4V reference alloy showed a homogeneous grain distribution. This homogeneity made it difficult to observe distinctive microstructural features with optical microscopy. Across all alloy samples, including Ti-6Al-4V, pores and surface contaminants such as carbon deposits were visible, indicating some level of surface imperfection.
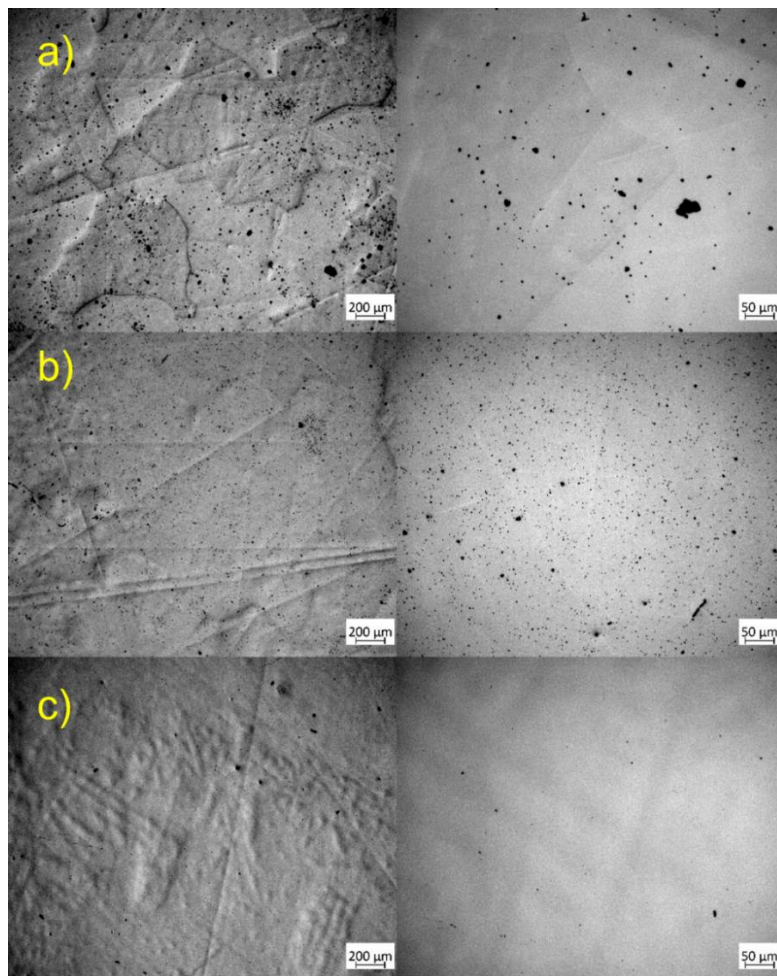
Figure 4. Optical micrographs of the Ti-Zr-Nb-Ta alloys a)Ti-40Zr-4Nb-33Ta b)Ti-30Z-4Nb-33Ta c)Ti-20Zr-4Nb-33Ta

9
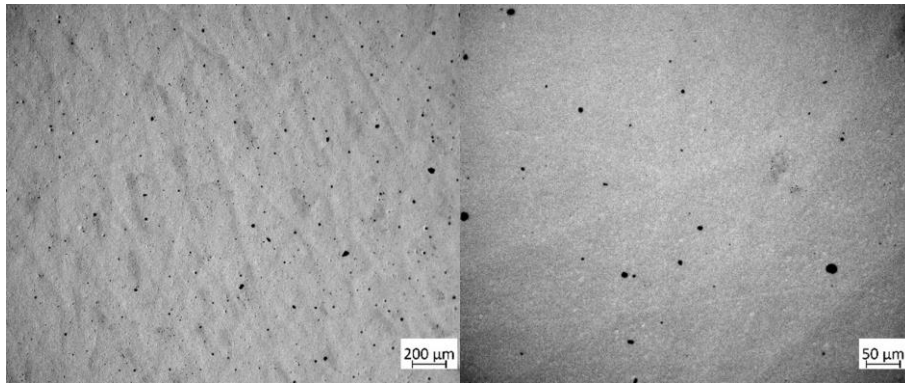
Figure 5. Optical microscopy image of Ti-6Al-4V
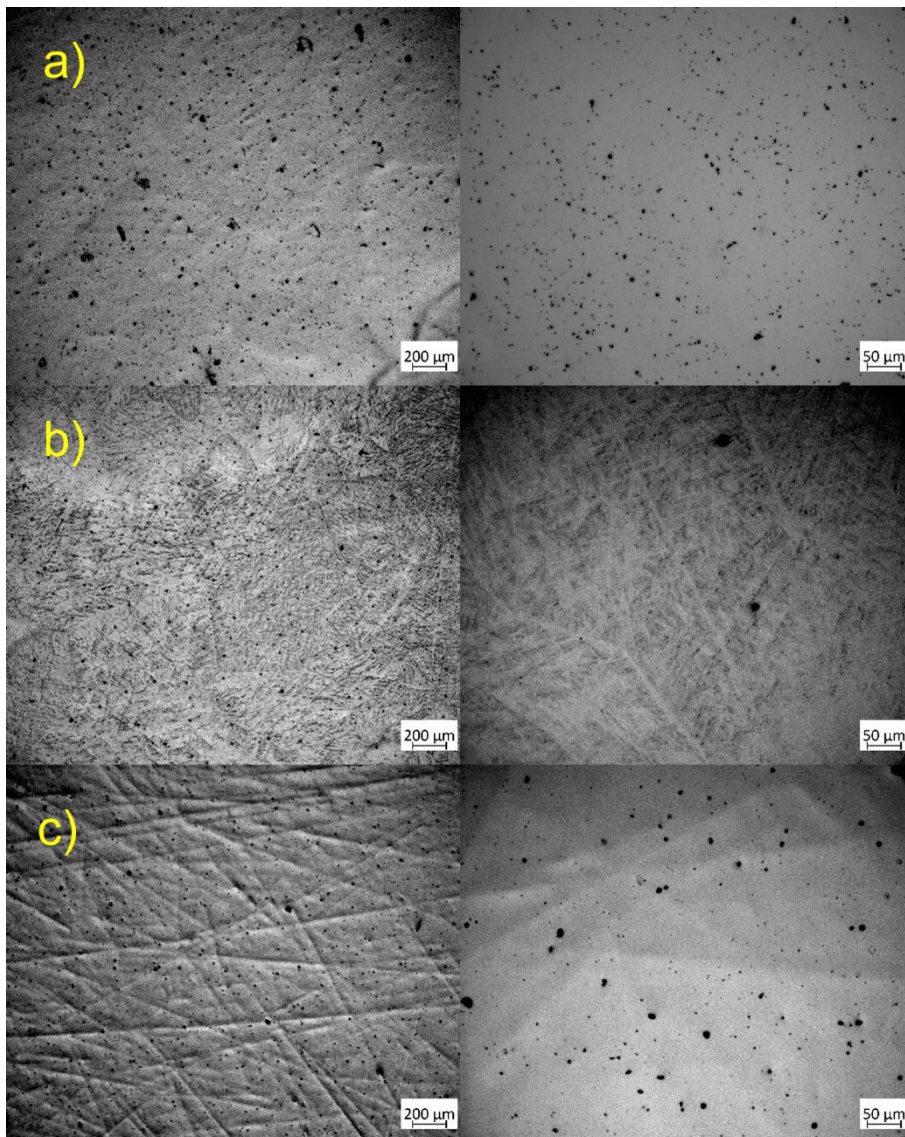
Figure 6. Optical micrographs of the Ti-Zr-Nb-Mo alloys a)Ti-30Zr-4Nb-10Mo b)Ti-30Z-4Nb-13Mo c)Ti-30Zr-4Nb-16Mo

4.1.2 Scanning Electron Microscopy (SEM), Energy Dispersive X-ray Spectroscopy (EDS)

Each titanium alloy sample was subjected to EDS analysis at four specific spots to capture localized variations in elemental composition. Additionally, one larger area was analyzed to obtain a more general overview of the elemental distribution across the sample. Figure 7 represents the EDS spectrum for Ti-40Zr-4Nb-33Ta. Peaks in the spectra correspond to the characteristic energies of X-rays emitted by the elements present in the samples, with the height of each peak indicating the relative abundance of the corresponding element. The remaining EDS spectra for the Ti-Zr-Nb-Ta, Ti-Zr-Nb-Mo, and Ti-6Al-4V alloys can be found in Appendice 6 and Appendice 7.
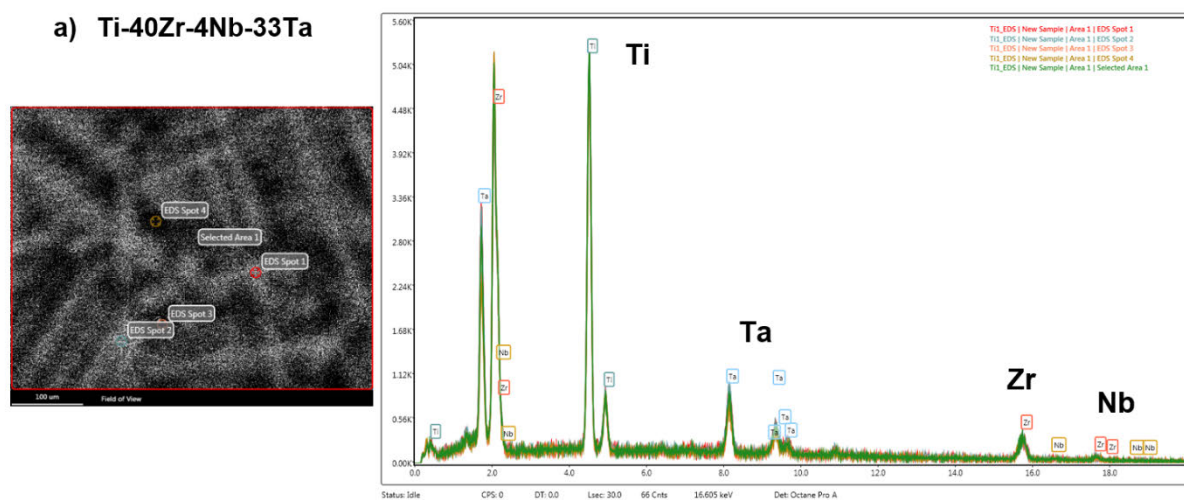
Figure 7. EDS spectrum for Ti-40Zr-4Nb-33Ta showing main peak of material composition

The chemical composition of the titanium alloys is despicted in Table 1,Table 2, Table 3

Table 1. Chemical composition of Ti-Zr-Nb-Ta alloys

Element	Ti-40Zr-4Nb-33Ta	Ti-30Zr-4Nb-33Ta	Ti-20Zr-4Nb-33Ta
Ti (wt%)	30.9	41.22	52.71
Ta (wt%)	18.64	22.67	19.37
Zr (wt%)	44.56	31.06	21.98
Nb (wt%)	4.1	5.04	5.93

Table 2. Chemical composition of Ti-Zr-Nb-Mo alloys

Element	Ti-30Zr-4Nb-10Mo	Ti-30Zr-4Nb-13Mo	Ti-30Zr-4Nb-16Mo
Zr (wt%)	26.32	26.6	27.76
Ti (wt%)	62.47	59.1	51.8
Nb (wt%)	4.02	8.34	5.2
Mo (wt%)	7.19	5.96	15.24

Table 3. Chemical composition Ti-6Al-4V

Element	Ti-6Al-4V
Al (wt%)	5.4
Ti (wt%)	90.98
V (wt%)	3.62

The BSE-SEM images of the titanium alloys reveal a characteristic dendritic microstructure as presented in Figure 8 and Figure 9. This is evident from the light-gray contrast of the dendrites and the dark-gray contrast of the inter-dendritic regions, indicating the redistribution of the constituent elements during solidification[9]. In Figure 8 The dendritic region (light-gray) contained a high concentration of Ta because of its higher melting point. In contrast, the inter-dendritic region (dark-gray) was enriched with Zr and Nb, owing to their lower melting points.
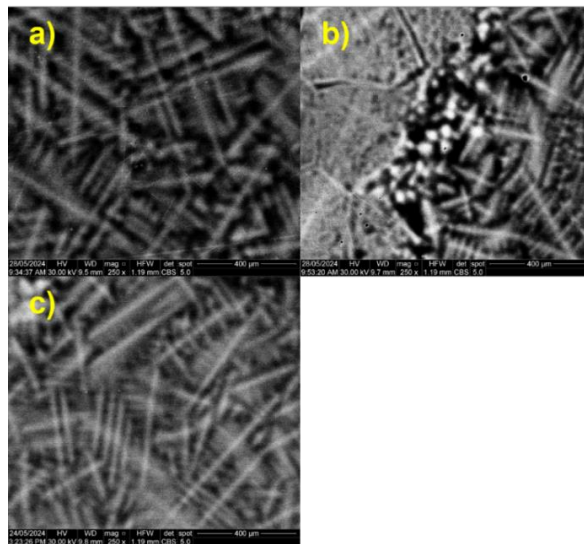
Figure 8. BSE-SEM images of the as-cast Ti-Zr-Nb-Ta alloys a)Ti-40Zr-4Nb-33Ta b)Ti-30Zr-4Nb-33Ta c)Ti-20Zr-4Nb-33Ta
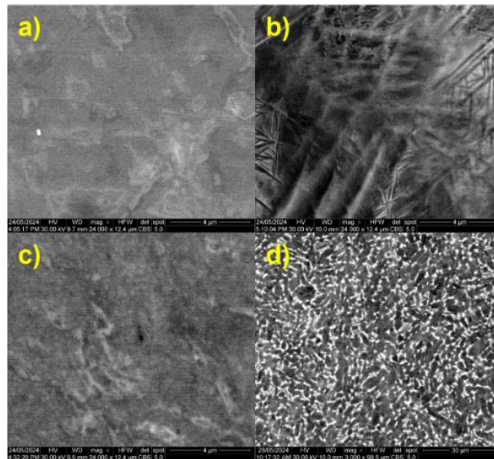
Figure 9. BSE-SEM images of the as-cast Ti-Zr-Nb-Mo alloys a)Ti-30Zr-4Nb-10Mo b)Ti-30Zr-4Nb-13Mo c)Ti-30Zr-4Nb-10Mo d)Ti-6Al-4V

4.2 Mechanical Testing

4.2.1 Nanohardness

Figure 10 shows the representative load-displacement curves obtained from the nanoindentation tests on the titanium alloys. These curves illustrate the relationship between the applied load and the penetration depth of the indenter. The nanoindentation curves display distinct loading and unloading segments. The slope of the initial unloading segment was used to calculate the elastic modulus, while the maximum load and corresponding penetration depth were used to determine the hardness following the equations (1) (2) (3) (4). The summary of the value of hardness (H) and Young's modulus (E) can be found in Appendice 8.
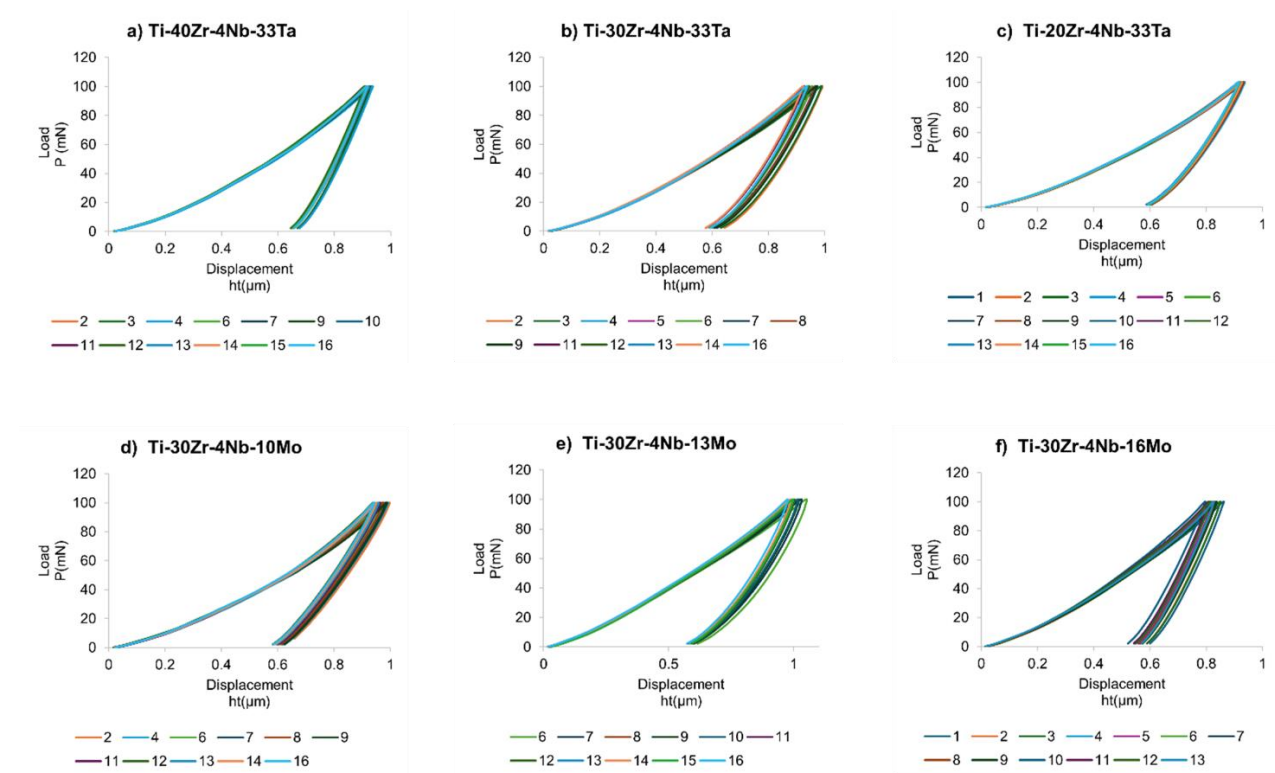
Figure 10. Representative load (P)–displacement (ht) nanoindentation curves for Ti-Zr-Nb-Ta and Ti-Zr-Nb-Mo alloys

The nanohardness values of the tested alloys exhibit a range from 3.9 to 5.3 GPa, with Ti-30Zr-4Nb-13Mo demonstrating the lowest hardness and Ti-30Zr-4Nb-16Mo showing the highest as presented in Figure 11. Ti-40Zr-4Nb-33Ta (H = 4.4 ± 0.09 GPa) and Ti-20Zr-4Nb-33Ta (H = 4.5 ± 0.07 GPa) exhibit similar hardness values, indicating that variations in Zr content (from 20wt% to 40wt%) have a modest effect on the nanohardness. Ti-30Zr-4Nb-33Ta (H = 4.2 ± 0.17 GPa) shows a slightly lower hardness compared to the other Ta-containing alloys, suggesting a potential influence of the intermediate Zr content on the microstructural characteristics affecting hardness.

Observing the trend in the Ti-Zr-Nb-Mo alloys, it is evident that an increase in Mo content generally correlates with an increase in nanohardness. This trend aligns with the previous EDS results showing that the alloy Ti-30Zr-4Nb-13Mo actually contains less Mo by weight than the alloy Ti-30Zr-4Nb-10Mo. The measured hardness values were Ti-30Zr-4Nb-13Mo (H = 3.9 ± 0.15 GPa), Ti-30Zr-4Nb-10Mo (H = 4.4 ± 0.16 GPa), and Ti-30Zr-4Nb-16Mo (H = 5.3 ± 0.24 GPa). This increase could be attributed to the solid-solution strengthening effect of Mo and the potential formation of harder phases.
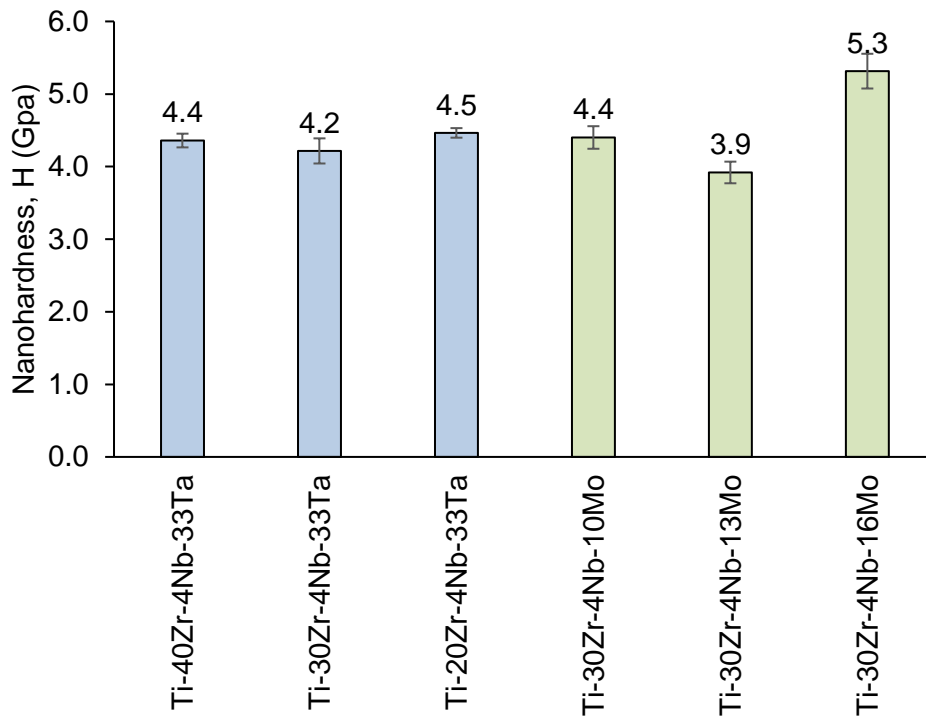
Figure 11. Nanohardness of Ti-Zr-Nb-Ta and Ti-Zr-Nb-Mo alloys

For biomedical applications, it is desirable for Young's modulus to closely match that of human bones (10–30 GPa) to reduce the stress-shielding effect. The Young's modulus of the Ti-Zr-Nb-Ta and Ti-Zr-Nb-Mo alloys are shown in Figure 12. For comparison, the Young's modulus of the widely used titanium alloy Ti-6Al-4V, was referenced from the thesis project 'Development of Novel Antibacterial Ti-Nb-Ga Alloys with Low Stiffness for Medical Implant Applications.' as the material was tested under the same conditions.

Among the Ta-containing alloys, increasing the Zr content from 20% to 40% resulted in variations in Young's modulus. Specifically, Ti-20Zr-4Nb-33Ta (E = 89 ± 0.89 GPa) and Ti-40Zr-4Nb-33Ta (E = 97 ± 1.13 GPa) showed higher module compared to Ti-30Zr-4Nb-33Ta (E = 82 ± 3.49 GPa).

14

In the Mo-containing alloys, an increase in Mo content generally correlated with an increase in Young's modulus. However, the EDS results revealed that Ti-30Zr-4Nb-13Mo actually contains less Mo by weight than Ti-30Zr-4Nb-10Mo. Despite this, Ti-30Zr-4Nb-13Mo (E = 73 ± 2.1 GPa) exhibited a slightly higher modulus than Ti-30Zr-4Nb-10Mo (E = 70 ± 2.5 GPa). Ti-30Zr-4Nb-16Mo (E = 108 ± 1.77 GPa) showed a significant increase in modulus, indicating that higher Mo content generally stiffens the alloy. Overall, all six tested alloys exhibited lower Young's modulus than Ti-6Al-4V (E=120 ± 2.32 GPa).
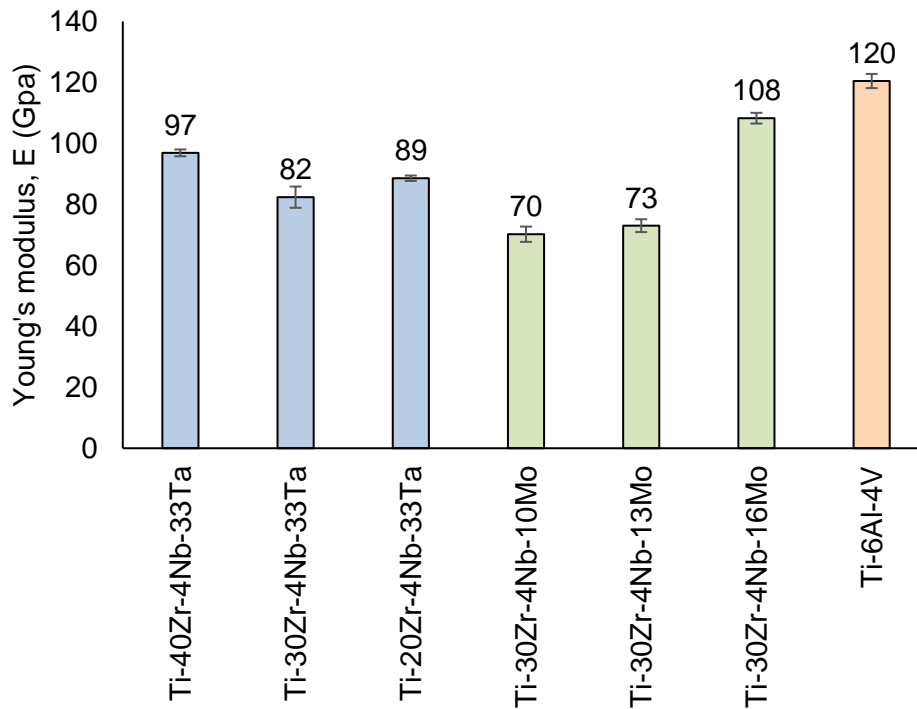
Figure 12. Young modulus of Ti-Zr-Nb-Ta and Ti-Zr-Nb-Mo alloys and commercial Ti-6Al-4V

4.2.2 Microhardness

The micro-hardness of the experimental Ti-Zr-Nb-Ta, Ti-Zr-Nb-Mo and Ti-6Al-4V alloys is shown in Figure 13. Notably, both Ti-30Zr-4Nb-10Mo (328±7.21) and Ti-30Zr-4Nb-13Mo (332±10.53) exhibit higher Vickers hardness values compared to the widely used Ti-6Al-4V alloy (300±1.77). In the Ti-Zr-Nb-Ta alloy series, a clear trend is observed where increasing the zirconium (Zr) content results in a decrease in hardness from 290 ± 9.26 for Ti-20Zr-4Nb-33Ta, 285 ± 5.22 for Ti-30Zr-4Nb-33Ta and 269 ±2.62 for Ti-40Zr-4Nb-33Ta. In the Mo-containing alloys, the hardness increases from 328 ± 7.21 for the Ti-30Zr-4Nb-10Mo alloy to 332 ± 10.53 for the Ti-30Zr-4Nb-13Mo alloy, indicating that a moderate increase in Mo content leads to a slight increase in hardness. However, EDS results revealed that the Ti-30Zr-4Nb-13Mo alloy actually contains less Mo by weight than the Ti-30Zr-4Nb-10Mo

alloy. When the Mo content is further increased to 16 wt%, the hardness significantly decreases to 268 ± 2.33. The values of the microhardness can be found in Appendice 9.
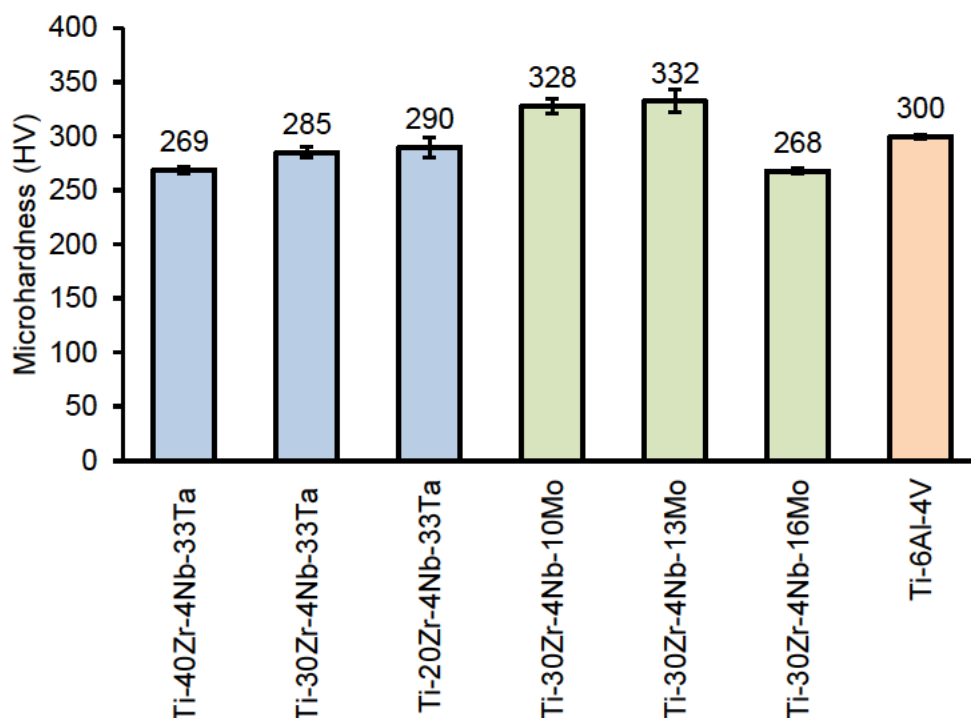
Figure 13. Micro-hardness of experimental Ti-Zr-Nb-Ta and Ti-Zr-Nb-Mo alloys and commercial Ti-6Al-4V

4.2.3 Tribocorrosion test at OCP

The evolution of the open circuit potential (OCP) over time for the titanium alloys was monitored before, during, and after sliding, as shown in Figure 14 and Figure 15. Three main regions can be identified. The first region, until 300 seconds, indicates the stabilization of the OCP potential. Prior to the initiation of sliding, the OCPs measured for all the alloys remained stable. At 300 seconds, the second region begins, where sliding occurs under nominal normal loads of 6 N, 17.5 N, and 30.8 N. An immediate sharp decline in potential is observed in all alloys, indicating surface depassivation caused by the mechanical removal of the passive film and the exposure of fresh, active titanium to the electrolyte[39]. Generally, during sliding, tribological stresses remove the passive film from the contact areas between the pin and the metallic sample, creating highly reactive regions within the wear track, unlike the less reactive areas outside the wear zone. The potential value observed during sliding (Ewear) results from the galvanic interaction between the depassivated wear track, which acts as a local anode, and the adjacent large passive unworn area, which acts as a cathode [40]. Throughout the sliding process, the OCP remains almost constant, suggesting that the wear track stays in a depassivated state. In the third phase, at 1665 seconds, sliding stops,

16

leading to an increase in the potential of all titanium alloys, approaching values similar to those recorded before sliding began. The increase in post-sliding potentials could be attributed to the accumulation of wear debris on the wear track and the thickening of the passive film outside the wear track, resulting from accelerated mass transport during the sliding process [40].
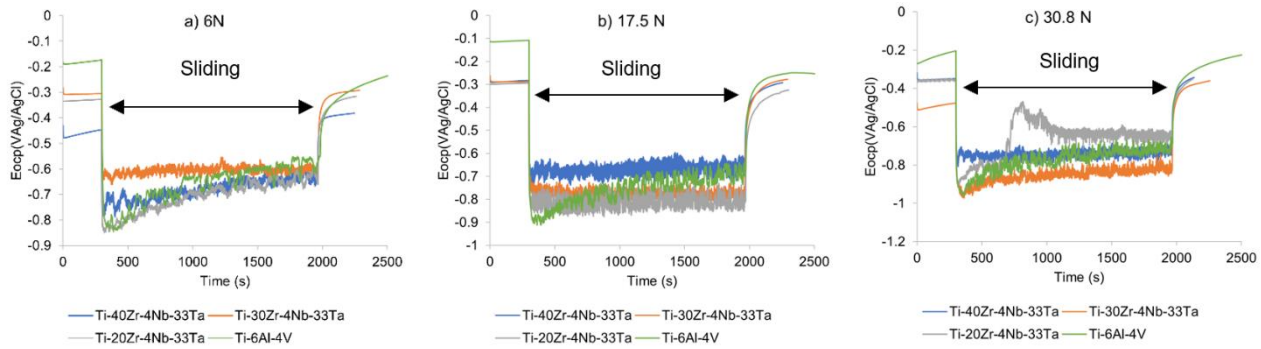
Figure 14. Time-Dependent OCP Changes during Sliding of a Smooth Zirconia Ball against Ti-Zr-Nb-Ta Alloys and Ti-6Al-4V at a) 6N, b) 17.5N, and c) 30.8N in PBS
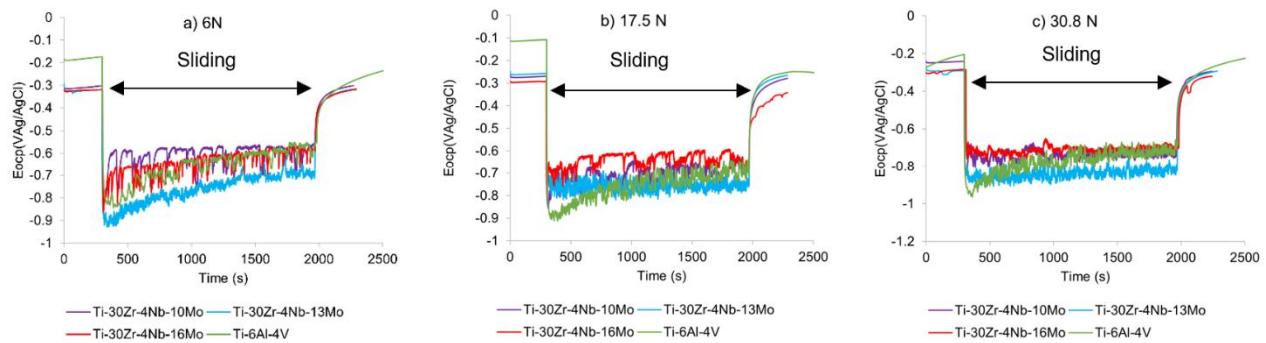
Figure 15. Time-Dependent OCP Changes during Sliding of a Smooth Zirconia Ball against Ti-Zr-Nb-Mo alloys and Ti-6Al-4V a)6N b)17.5N and c)30.8N in PBS

The electrochemical parameters determined from the OCP curves potential before sliding E_{OCP} , during sliding (E_{wear}), potential drop ($|\Delta E|$) can be found in Appendice 10 for Ti-Zr-Nb-Ta alloys and Appendice 11 for Ti-Zr-Nb-Mo alloys. The SEM observations of the wear tracks on the Ti-30Zr-4Nb-16Mo alloy at two different force levels, 17.5 N and 30.8 N, reveal significant differences in wear mechanisms and track morphology. At 17.5 N, the wear track shows relatively shallow and uniform grooves along the sliding direction, indicating mild abrasive wear with minor plastic deformation and some scattered wear debris. In contrast, at 30.8 N, the wear track exhibits deeper and more pronounced grooves, reflecting increased abrasive wear. The higher magnifications reveal significant plastic deformation, larger amounts of wear debris, and more prominent surface roughness at the higher force.

The transition from 17.5 N to 30.8 N results in a noticeable increase in wear severity, with deeper grooves and more substantial surface deformation at the higher load as presented in Figure 17
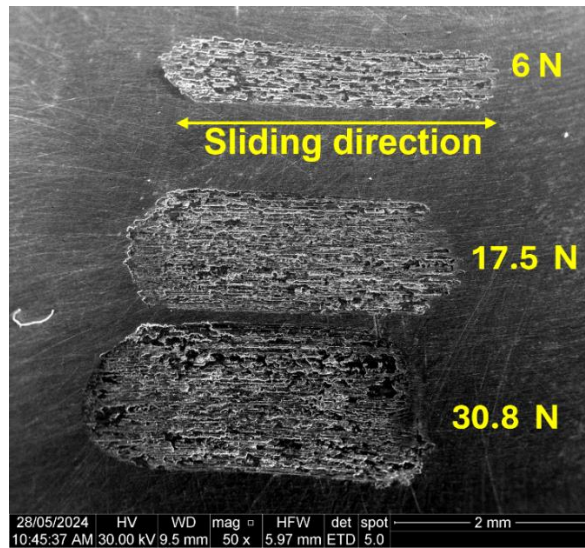
Figure 16. Morphological characteristic of the wear tracks of Ti-30Zr-4Nb-16Mo under OCP conditions
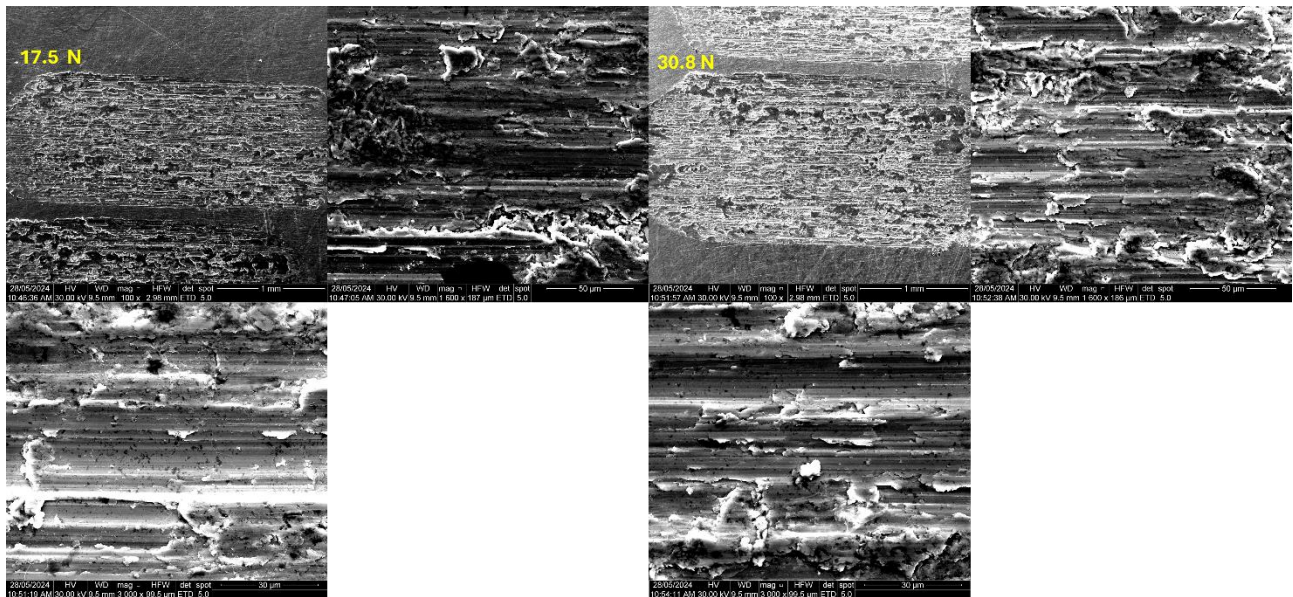
Figure 17. SEM analysis of the wear track for Ti-30Zr-4Nb-16Mo at 17.5 N and 30.8 N

5   CHAPTER FOUR: DISCUSSION

As per Achard's law[32] , there is a direct correlation between a material's wear resistance and hardness, indicating that increasing the material's hardness can enhance its ability to withstand compressive deformation and improve its resistance to wear. This principle is supported by the findings of this study. During the nanoindentation test, the Ti-30Zr-4Nb-

18

16Mo alloy exhibited the highest nanohardness value of 5.3 ± 0.24 GPa, which is higher than the 5.0 ± 0.1 GPa reported for Ti-6Al-4V[41] . Additionally, in the tribocorrosion test at OCP, the Ti-30Zr-4Nb-16Mo alloy consistently showed the lowest E_{wear} values at higher forces, specifically -642.31 mV ± 33 at 17.5N and -709.07 mV ± 42 at 30.8N. This superior performance at higher force levels aligns with Achard's law, reinforcing the idea that the increased hardness of Ti-30Zr-4Nb-16Mo contributes to its enhanced wear resistance. In Ta-containing alloys, notable variations in performance were observed across different applied force levels (6N, 17.5N, and 30.8N). The Ti-30Zr-4Nb-33Ta alloy showed the lowest E_{wear} value of -604.73 mV± 15 at 6N, indicating superior wear resistance at this force level. At 17.5N, the Ti-40Zr-4Nb-33Ta alloy exhibited an E_{wear} value of -674.28 mV±22, suggesting it performed best under this force condition. Similarly, at 30.8N, the Ti-20Zr-4Nb-33Ta alloy demonstrated the lowest E_{wear} value of -666.55 mV±106, highlighting its optimal performance at this higher force level. In Mo-containing alloys, at 6N, the Ti-30Zr-4Nb-10Mo alloy exhibited the lowest E_{wear} of -614.22 mV±54, indicating superior wear resistance at this force level. At higher forces, specifically at 17.5N and 30.8N, the Ti-30Zr-4Nb-16Mo alloy consistently showed the lowest E_{wear} values of -642.31 mV±33 and -709.07 mV±42, respectively, demonstrating its superior performance at these force levels. Overall, across 21 experiments, both Ti-Zr-Nb-Ta and Ti-Zr-Nb-Mo alloys exhibited superior wear resistance compared to Ti-6Al-4V. In comparison to the Ta-containing alloys, Ti-6Al-4V exhibits the highest potential drop **|ΔE|** among the tested alloys (658.03 mV at 17.5 N), indicating greater susceptibility to corrosion or changes in electrochemical behavior. A similar trend is observed when comparing with Mo-containing alloys, where Ti-6Al-4V also shows the highest potential drop (658.03 mV at 17.5 N).The measured microhardness value of the reference alloy Ti-6Al-4V (300 HV±1.77) deviates around 2% of that reported by[33] (294 HV).The lower microhardness value of the highest Mo sample Ti-30Zr-4Nb-16Mo (268 HV±2.33) compared with the two alloys containing less Mo, Ti-30Zr-4Nb-10Mo (328 HV±7.21) and Ti-30Zr-4Nb-13Mo (332 HV±10.53); matches with the results of [33] were the alloys containing more than 15wt% Mo had a lower microhardness value than the ones with Mo contain between 10 - 13wt%. The interpretation of the microhardness values on the three measured Ti alloys containing Mo can be complex due to multiple effects such as strain aging, grain size, crystal structure among others. As mentioned by[33], transition between phases can occur, and create strains that can cause the structure to be less hardened. This could help explain the lower microhardness values on the high Mo-containing sample.Different authors have reported an increase in the microhardness values as the Zr content increases in Ti-Zr alloys[42] [43], however, the results show a decrease in the HV

values as the Zr content increases, going from 269 HV±2.62 for the Ti-40Zr-4Nb-33Ta to 290HV±9.26 for the Ti-20Zr-4Nb-33Ta alloy. The reason behind this behaviour is not certain at this point.The elasticity module observed vary across the three Zr alloys tested from 82 to 97 Gpa, which is lower than the one found on the Ti-6Al-4V, 120 Gpa as tested and 124 Gpa as reported at [44] . The elastic modulus increased as the wt% of Mo increased, going from 70 to 108 GPa, lower than the as-tested 120 GPa of Ti-6Al-4V. Different authors[42], [43], [45] have described how different atomic radii of the elements present in the alloy, can influence lattice distortion and the degrees of supersaturation, this can result in a change in the distance between atoms and consequently, a variation in the elasticity modulus. In this case, the Zr and Ta have a larger atomic radius than Ti, while the Nb has a smaller atomic radius.

6 CHAPTER FIVE: CONCLUSIONS AND FUTURE WORK

An in-depth comparative study was conducted to analyze the microstructure, mechanical properties, and tribocorrosion behavior in a PBS solution of six newly designed as-cast titanium alloys, along with the widely used commercial Ti–6Al–4V alloy. This research aimed to evaluate and compare these materials to determine their suitability for biomedical applications. The summarized properties and detailed findings are presented in Table 4:

Table 4. Summarized mechanical properties for Ti-Zr-Nb-Ta, Ti-Zr-Nb-Mo and Ti-6Al-4V alloys

Sample	H (Gpa)	E (Gpa)	HV	E_{wear} (mV vs Ag|AgCl)		
				6 N	17.5 N	30 N
Ti-40Zr-4Nb-33Ta	4.4 ± 0.09	97 ± 1.13	269 ± 2.62	-688.06	**-674.28**	-744.12
Ti-30Zr-4Nb-33Ta	4.2 ± 0.17	82 ± 3.49	285 ± 5.22	**-604.73**	-774.50	-860.83
Ti-20Zr-4Nb-33Ta	4.5 ± 0.07	89 ± 0.89	290 ± 9.26	-721.04	-815.17	**-666.55**
Ti-6Al-4V	5.0 ± 0.1	120 ± 2.32	300 ± 1.77	-678.09	-769.87	-786.77
Ti-30Zr-4Nb-10Mo	4.4 ± 0.16	70 ± 2.50	328 ± 7.21	**-614.22**	-705.73	-740.05
Ti-30Zr-4Nb-13Mo	3.9 ± 0.15	73 ± 2.10	332 ± 10.53	-777.79	-757.86	-844.36
Ti-30Zr-4Nb-16Mo	5.3 ± 0.24	108 ± 1.77	268 ± 2.33	-649.94	**-642.31**	**-709.07**
Ti-6Al-4V	5.0 ± 0.1	120 ± 2.32	300 ± 1.77	-678.09	-769.87	-786.77

Optical microscopy of the Ti-Zr-Nb-Ta, Ti-Zr-Nb-Mo, and Ti-6Al-4V alloys revealed homogeneous grain structures, with surface imperfections such as pores and carbon deposits visible across all samples. The lack of distinct grain structures at the magnifications used indicates challenges in microstructural analysis using this technique.The

nanoindentation tests showed a range of nanohardness values from 3.9 to 5.3 GPa. Ti-30Zr-4Nb-16Mo exhibited the highest nanohardness (5.3 ± 0.24 GPa), indicating its superior mechanical properties. The results suggest that Mo content positively influences the hardness of the alloys, with higher Mo content leading to increased hardness due to solid-solution strengthening and potential formation of harder phases. Among the β-type titanium alloys, an improved wear resistance with lower damage was remarked for Ti-30Zr-4Nb-16Mo, attributed to its increased nanohardness.The Young's modulus of all the tested alloys was significantly lower than that of Ti-6Al-4V (E=120 ± 2.32 GPa), ranging from 70 to 108 GPa. Ti-30Zr-4Nb-13Mo (73 ± 2.1 GPa) and Ti-30Zr-4Nb-10Mo (70 ± 2.5 GPa) demonstrated lower modulus values, closer to the desirable range for biomedical applications. The Ti-30Zr-4Nb-16Mo alloy exhibited the highest modulus (108 ± 1.77 GPa), highlighting the impact of higher Mo content.The tribocorrosion tests at OCP revealed significant differences in wear resistance among the alloys at various force levels. For the Ta-containing alloys Ti-30Zr-4Nb-33Ta demonstrated the lowest E_{wear} at 6N, Ti-40Zr-4Nb-33Ta at 17.5N, and Ti-20Zr-4Nb-33Ta at 30.8N, indicating optimal performance under these specific conditions. For Mo-containing alloys, Ti-30Zr-4Nb-10Mo exhibited the lowest E_{wear} at 6N, while Ti-30Zr-4Nb-16Mo consistently showed superior performance at higher forces (17.5N and 30.8N).Overall, this study demonstrates that the novel Ti-Zr-Nb-Ta and Ti-Zr-Nb-Mo alloys possess promising mechanical and tribocorrosion properties, making them suitable candidates for biomedical implant applications. The improved wear resistance and lower Young's modulus compared to Ti-6Al-4V indicate their potential to reduce the stress-shielding effect and enhance implant longevity. The findings provide a foundation for the future application of these novel alloys in biomedical devices, with the potential to significantly improve patient outcomes by reducing the frequency of replacement surgeries. To build on the findings of this study, several areas of future work are recommended. For improved visibility of the microstructure, electrolytic polishing is suggested to achieve clearer grain structure visibility. This can be followed by chemical etching using Kroll's or Weck's reagent to enhance the contrast of the β phase and other microstructural features. Comprehensive biocompatibility studies, including cytotoxicity, cell adhesion, and in-vivo tests, are essential to evaluate the potential of these alloys for medical implant applications. Lastly, the effects of surface treatments and coatings on the mechanical and tribological properties of the alloys should be evaluated to enhance their performance in biomedical applications.

7 REFERENCES

[1]   Q. Chen and G. A. Thouas, "Metallic implant biomaterials," *Materials Science and Engineering R: Reports*, vol. 87, pp. 1–57, 2015, doi: 10.1016/j.mser.2014.10.001.

[2]   M. Sarraf, E. Rezvani Ghomi, S. Alipour, S. Ramakrishna, and N. Liana Sukiman, "A state-of-the-art review of the fabrication and characteristics of titanium and its alloys for biomedical applications," *Bio-Design and Manufacturing*, vol. 5, no. 2. Springer, pp. 371–395, Apr. 01, 2022. doi: 10.1007/s42242-021-00170-3.

[3]   M. Niinomi, "Recent Metallic Materials for Biomedical Applications," pp. 477–486, 2002, doi: https://doi.org/10.1007/s11661-002-0109-2.

[4]   A. N. Omran, M. M. Ali, and M. M. Kh, "Biocompatibility, corrosion, and wear resistance of β titanium alloys for biomedical applications," *Appl Phys A Mater Sci Process*, vol. 126, no. 12, Dec. 2020, doi: 10.1007/s00339-020-04118-9.

[5]   M. Kaur and K. Singh, "Review on titanium and titanium based alloys as biomaterials for orthopaedic applications," *Materials Science and Engineering C*, vol. 102. Elsevier Ltd, pp. 844–862, Sep. 01, 2019. doi: 10.1016/j.msec.2019.04.064.

[6]   J. M. Cordeiro and V. A. R. Barão, "Is there scientific evidence favoring the substitution of commercially pure titanium with titanium alloys for the manufacture of dental implants?," *Materials Science and Engineering C*, vol. 71. Elsevier Ltd, pp. 1201–1215, Feb. 01, 2017. doi: 10.1016/j.msec.2016.10.025.

[7]   N. Siony, L. Vuong, O. Lundaajamts, and S. Kadkhodaei, "Computational Design of Corrosion-resistant and Wear-resistant Titanium Alloys for Orthopedic Implants," Sep. 2022, doi: 10.1016/j.mtcomm.2022.104465.

[8]   M. Geetha, A. K. Singh, R. Asokamani, and A. K. Gogia, "Ti based biomaterials, the ultimate choice for orthopaedic implants - A review," *Progress in Materials Science*, vol. 54, no. 3. pp. 397–425, May 2009. doi: 10.1016/j.pmatsci.2008.06.004.

[9]   Z. Li, W. Lai, X. Tong, D. You, W. Li, and X. Wang, "Design of TiZrNbTa multi-principal element alloys with outstanding mechanical properties and wear resistance," *Materials Science and Engineering: A*, vol. 845, Jun. 2022, doi: 10.1016/j.msea.2022.143203.

[10] M. Mohammed, Z. Khan, and A. Siddiquee, "Beta Titanium Alloys The Lowest Elastic Modulus for biomedical applications a review," *International Journal of Chemical, Nuclear, Metallurgical and Materials Engineering*, vol. 8, 2014.

[11] X. Zhao, M. Niinomi, M. Nakai, T. Ishimoto, and T. Nakano, "Development of high Zr-containing Ti-based alloys with low Young's modulus for use in removable implants," *Materials Science and Engineering C*, vol. 31, no. 7, pp. 1436–1444, Oct. 2011, doi: 10.1016/j.msec.2011.05.013.

[12] M. H. C. Tan, A. D. Baghi, R. Ghomashchi, W. Xiao, and R. H. Oskouei, "Effect of niobium content on the microstructure and Young's modulus of Ti-xNb-7Zr alloys for medical implants," *J Mech Behav Biomed Mater*, vol. 99, pp. 78–85, Nov. 2019, doi: 10.1016/j.jmbbm.2019.07.014.

[13] P. Vizureanu, S. Bălțatu, and A. V. Sandu, "Development of New Advanced Ti-Mo Alloys for Medical Applications," 2020. doi: 10.5772/intechopen.91906.

[14] W. Weng, A. Biesiekierski, J. Lin, S. Ozan, Y. Li, and C. Wen, "Development of beta-type Ti-Nb-Zr-Mo alloys for orthopedic applications," *Appl Mater Today*, vol. 22, Mar. 2021, doi: 10.1016/j.apmt.2021.100968.

[15] M. Niinomi *et al.*, "Corrosion wear fracture of new b type biomedical titanium alloys," 1999.

[16] I. Simsek and D. Ozyurek, "Investigation of the wear and corrosion behaviors of Ti5Al2.5Fe and Ti6Al4V alloys produced by mechanical alloying method in simulated body fluid environment," *Materials Science and Engineering C*, vol. 94, pp. 357–363, Jan. 2019, doi: 10.1016/j.msec.2018.09.047.

[17] C. Ohkubo *et al.*, "Wear resistance of experimental Ti-Cu alloys," *Biomaterials*, vol. 24, no. 20, pp. 3377–3381, 2003, doi: 10.1016/S0142-9612(03)00157-1.

[18] M. O. Alam and A. S. M. A. Haseeb, "Response of Ti-6Al-4V and Ti-24Al-11Nb alloys to dry sliding wear against hardened steel," 2002. [Online]. Available: www.elsevier.com/locate/triboint

[19] A. C. L. Faria, R. C. S. Rodrigues, A. P. R. A. Claro, M. da G. C. de Mattos, and R. F. Ribeiro, "Wear resistance of experimental titanium alloys for dental applications," *J*

Mech Behav Biomed Mater, vol. 4, no. 8, pp. 1873–1879, Nov. 2011, doi: 10.1016/j.jmbbm.2011.06.004.

[20] W. T. Qu, X. G. Sun, B. F. Yuan, K. M. Li, Z. G. Wang, and Y. Li, "Tribological behaviour of biomedical Ti–Zr-based shape memory alloys," *Rare Metals*, vol. 36, no. 6, pp. 478–484, Jun. 2017, doi: 10.1007/s12598-017-0882-0.

[21] V. G. Pina, V. Amigó, and A. I. Muñoz, "Microstructural, electrochemical and tribo-electrochemical characterisation of titanium-copper biomedical alloys," *Corros Sci*, vol. 109, pp. 115–125, Aug. 2016, doi: 10.1016/j.corsci.2016.02.014.

[22] L. M. Kang and C. Yang, "A Review on High-Strength Titanium Alloys: Microstructure, Strengthening, and Properties," *Advanced Engineering Materials*, vol. 21, no. 8. Wiley-VCH Verlag, Aug. 01, 2019. doi: 10.1002/adem.201801359.

[23] M. Delshadmanesh, G. Khatibi, M. Z. Ghomsheh, M. Lederer, M. Zehetbauer, and H. Danninger, "Influence of microstructure on fatigue of biocompatible β-phase Ti-45Nb," *Materials Science and Engineering: A*, vol. 706, pp. 83–94, Oct. 2017, doi: 10.1016/j.msea.2017.08.098.

[24] S. Ehtemam-Haghighi, K. G. Prashanth, H. Attar, A. K. Chaubey, G. H. Cao, and L. C. Zhang, "Evaluation of mechanical and wear properties of Ti[sbnd]xNb[sbnd]7Fe alloys designed for biomedical applications," *Mater Des*, vol. 111, pp. 592–599, Dec. 2016, doi: 10.1016/j.matdes.2016.09.029.

[25] L. J. Xu, S. L. Xiao, J. Tian, and Y. Y. Chen, "Microstructure, mechanical properties and dry wear resistance of β-type Ti-15Mo-xNb alloys for biomedical applications," *Transactions of Nonferrous Metals Society of China (English Edition)*, vol. 23, no. 3, pp. 692–698, Mar. 2013, doi: 10.1016/S1003-6326(13)62518-2.

[26] Z. Gölbaşı, B. Öztürk, S. E. Sünbül, and K. İçin, "Mechanical, wear and corrosion behavior of Ti–6Al–xNb (x = 3.5–21 wt%) alloys manufactured by powder metallurgy," *Powder Technol*, vol. 426, Aug. 2023, doi: 10.1016/j.powtec.2023.118696.

[27] A. K. Pandey, R. K. Gautam, and C. K. Behera, "Corrosion and wear behavior of Ti–5Cu-xNb biomedical alloy in simulated body fluid for dental implant applications," *J Mech Behav Biomed Mater*, vol. 137, Jan. 2023, doi: 10.1016/j.jmbbm.2022.105533.

[28] L. J. Xu, S. L. Xiao, J. Tian, Y. Y. Chen, and Y. D. Huang, "Microstructure and dry wear properties of Ti-Nb alloys for dental prostheses," *Transactions of Nonferrous Metals Society of China (English Edition)*, vol. 19, no. SUPPL. 3, Dec. 2009, doi: 10.1016/S1003-6326(10)60124-0.

[29] A. Hynowska *et al.*, "Nanostructured β-phase Ti-31.0Fe-9.0Sn and sub-μm structured Ti-39.3Nb-13.3Zr-10.7Ta alloys for biomedical applications: Microstructure benefits on the mechanical and corrosion performances," *Materials Science and Engineering C*, vol. 32, no. 8, pp. 2418–2425, Dec. 2012, doi: 10.1016/j.msec.2012.07.016.

[30] T. Xiang *et al.*, "Phase-tunable equiatomic and non-equiatomic Ti-Zr-Nb-Ta high-entropy alloys with ultrahigh strength for metallic biomaterials," *J Mater Sci Technol*, vol. 117, pp. 196–206, Aug. 2022, doi: 10.1016/j.jmst.2021.12.014.

[31] S. Ozan, J. Lin, Y. Li, and C. Wen, "New Ti-Ta-Zr-Nb alloys with ultrahigh strength for potential orthopedic implant applications," *J Mech Behav Biomed Mater*, vol. 75, pp. 119–127, Nov. 2017, doi: 10.1016/j.jmbbm.2017.07.011.

[32] J. F. Archard, "Contact and rubbing of flat surfaces," *J Appl Phys*, vol. 24, no. 8, pp. 981–988, 1953, doi: 10.1063/1.1721448.

[33] W. Ho, C. Ju, and J. Chern Lin, "Structure and properties of cast binary Ti-Mo alloys," 1999, doi: https://doi.org/10.1016/S0142-9612(99)00114-3.

[34] N. Hua *et al.*, "Mechanical, corrosion, and wear properties of biomedical Ti–Zr–Nb–Ta–Mo high entropy alloys," *J Alloys Compd*, vol. 861, Apr. 2021, doi: 10.1016/j.jallcom.2020.157997.

[35] A. B. Elshalakany *et al.*, "Microstructure and Mechanical Properties of Ti-Mo-Zr-Cr Biomedical Alloys by Powder Metallurgy," *J Mater Eng Perform*, vol. 26, no. 3, pp. 1262–1271, Mar. 2017, doi: 10.1007/s11665-017-2531-z.

[36] M. Masanta, S. M. Shariff, and A. Roy Choudhury, "Evaluation of modulus of elasticity, nano-hardness and fracture toughness of TiB2-TiC-Al2O3 composite coating developed by SHS and laser cladding," *Materials Science and Engineering: A*, vol. 528, no. 16–17, pp. 5327–5335, Jun. 2011, doi: 10.1016/j.msea.2011.03.057.

[37] A. Hynowska *et al.*, "Nanostructured β-phase Ti-31.0Fe-9.0Sn and sub-μm structured Ti-39.3Nb-13.3Zr-10.7Ta alloys for biomedical applications: Microstructure benefits

on the mechanical and corrosion performances," *Materials Science and Engineering C*, vol. 32, no. 8, pp. 2418–2425, Dec. 2012, doi: 10.1016/j.msec.2012.07.016.

[38] S. Ehtemam-Haghighi, G. Cao, and L. C. Zhang, "Nanoindentation study of mechanical properties of Ti based alloys with Fe and Ta additions," *J Alloys Compd*, vol. 692, pp. 892–897, 2017, doi: 10.1016/j.jallcom.2016.09.123.

[39] V. G. Pina, A. Dalmau, F. Devesa, V. Amigó, and A. I. Muñoz, "Tribocorrosion behavior of beta titanium biomedical alloys in phosphate buffer saline solution," *J Mech Behav Biomed Mater*, vol. 46, pp. 59–68, Jun. 2015, doi: 10.1016/j.jmbbm.2015.02.016.

[40] L. A. Alberta *et al.*, "Tribocorrosion behavior of β-type Ti-Nb-Ga alloys in a physiological solution," *Tribol Int*, vol. 181, Mar. 2023, doi: 10.1016/j.triboint.2023.108325.

[41] A. Hynowska *et al.*, "Nanostructured β-phase Ti-31.0Fe-9.0Sn and sub-μm structured Ti-39.3Nb-13.3Zr-10.7Ta alloys for biomedical applications: Microstructure benefits on the mechanical and corrosion performances," *Materials Science and Engineering C*, vol. 32, no. 8, pp. 2418–2425, Dec. 2012, doi: 10.1016/j.msec.2012.07.016.

[42] D. R. N. Correa, F. B. Vicente, T. A. G. Donato, V. E. Arana-Chavez, M. A. R. Buzalaf, and C. R. Grandini, "The effect of the solute on the structure, selected mechanical properties, and biocompatibility of Ti-Zr system alloys for dental applications," *Materials Science and Engineering C*, vol. 34, no. 1, pp. 354–359, 2014, doi: 10.1016/j.msec.2013.09.032.

[43] W. F. Ho, W. K. Chen, S. C. Wu, and H. C. Hsu, "Structure, mechanical properties, and grindability of dental Ti-Zr alloys," *J Mater Sci Mater Med*, vol. 19, no. 10, pp. 3179–3186, Oct. 2008, doi: 10.1007/s10856-008-3454-x.

[44] Y. L. Zhou, M. Niinomi, and T. Akahori, "Effects of Ta content on Young's modulus and tensile properties of binary Ti-Ta alloys for biomedical applications," *Materials Science and Engineering: A*, vol. 371, no. 1–2, pp. 283–290, Apr. 2004, doi: 10.1016/j.msea.2003.12.011.

[45] P. Chui, R. Jing, F. Zhang, J. Li, and T. Feng, "Mechanical properties and corrosion behavior of β-type Ti-Zr-Nb-Mo alloys for biomedical application," *J Alloys Compd*, vol. 842, Nov. 2020, doi: 10.1016/j.jallcom.2020.155693.

[46] D. Kuroda, M. Niinomi, M. Morinaga, Y. Kato, and T. Yashiro, "Design and mechanical properties of new i type titanium alloys for implant materials," 1998.

[47] J. M. Chaves, O. Florêncio, P. S. Silva, P. W. B. Marques, and C. R. M. Afonso, "Influence of phase transformations on dynamical elastic modulus and anelasticity of beta Ti-Nb-Fe alloys for biomedical applications," *J Mech Behav Biomed Mater*, vol. 46, pp. 184–196, Jun. 2015, doi: 10.1016/j.jmbbm.2015.02.030.

[48] I. Kopova, J. Stráský, P. Harcuba, M. Landa, M. Janeček, and L. Bačákova, "Newly developed Ti-Nb-Zr-Ta-Si-Fe biomedical beta titanium alloys with increased strength and enhanced biocompatibility," *Materials Science and Engineering C*, vol. 60, pp. 230–238, Mar. 2016, doi: 10.1016/j.msec.2015.11.043.

[49] S. Ehtemam-Haghighi, Y. Liu, G. Cao, and L. C. Zhang, "Influence of Nb on the $\beta \rightarrow \alpha''$ martensitic phase transformation and properties of the newly designed Ti-Fe-Nb alloys," *Materials Science and Engineering C*, vol. 60, pp. 503–510, Mar. 2016, doi: 10.1016/j.msec.2015.11.072.

[50] Y. L. Hao, Z. B. Zhang, S. J. Li, and R. Yang, "Microstructure and mechanical behavior of a Ti-24Nb-4Zr-8Sn alloy processed by warm swaging and warm rolling," *Acta Mater*, vol. 60, no. 5, pp. 2169–2177, Mar. 2012, doi: 10.1016/j.actamat.2012.01.003.

[51] C. D. Rabadia *et al.*, "High-strength β stabilized Ti-Nb-Fe-Cr alloys with large plasticity," *Materials Science and Engineering: A*, vol. 732, pp. 368–377, Aug. 2018, doi: 10.1016/j.msea.2018.07.031.

[52] A. Yolun, M. Şimşek, M. Kaya, E. E. Annaç, M. Köm, and Ö. Çakmak, "Fabrication, characterization, and in vivo biocompatibility evaluation of titanium-niobium implants," *Proc Inst Mech Eng H*, vol. 235, no. 1, pp. 99–108, Jan. 2021, doi: 10.1177/0954411920960854.

[53] T. Sjafrizal, A. Dehghan-Manshadi, D. Kent, M. Yan, and M. S. Dargusch, "Effect of Fe addition on properties of Ti–6Al-xFe manufactured by blended elemental process," *J Mech Behav Biomed Mater*, vol. 102, Feb. 2020, doi: 10.1016/j.jmbbm.2019.103518.

[54] P. Xue, Y. Li, K. Li, D. Zhang, and C. Zhou, "Superelasticity, corrosion resistance and biocompatibility of the Ti-19Zr-10Nb-1Fe alloy," *Materials Science and Engineering C*, vol. 50, pp. 179–186, May 2015, doi: 10.1016/j.msec.2015.02.004.

[55] P. Wang, Y. Feng, F. Liu, L. Wu, and S. Guan, "Microstructure and mechanical properties of Ti-Zr-Cr biomedical alloys," *Materials Science and Engineering C*, vol. 51, pp. 148–152, 2015, doi: 10.1016/j.msec.2015.02.028.

[56] C. M. Lee, W. F. Ho, C. P. Ju, and J. H. Chern Lin, "Structure and properties of Titanium±25 Niobium±x iron alloys," *Journal of material science in medicine*, vol. 13, pp. 695–700, 2002.

[57] S. Griza, D. H. G. de Souza Sá, W. W. Batista, J. C. G. de Blas, and L. C. Pereira, "Microstructure and mechanical properties of hot rolled TiNbSn alloys," *Mater Des*, vol. 56, pp. 200–208, 2014, doi: 10.1016/j.matdes.2013.10.067.

[58] J. Wu *et al.*, "Development of biomedical Ti-Nb-Zr-Mn alloys with enhanced mechanical properties and corrosion resistance," *Mater Today Commun*, vol. 30, Mar. 2022, doi: 10.1016/j.mtcomm.2021.103027.

[59] P. Qi, B. Li, T. Wang, L. Zhou, and Z. Nie, "Microstructure and properties of a novel ternary Ti–6Zr–xFe alloy for biomedical applications," *J Alloys Compd*, vol. 854, Feb. 2021, doi: 10.1016/j.jallcom.2020.157119.

[60] M. S. Baltatu *et al.*, "Design, synthesis, and preliminary evaluation for ti-mo-zr-ta-si alloys for potential implant applications," *Materials*, vol. 14, no. 22, Nov. 2021, doi: 10.3390/ma14226806.

[61] W. F. Ho, S. C. Wu, H. W. Wang, and H. C. Hsu, "Effects of Cr addition on grindability of cast Ti-10Zr based alloys," *Mater Chem Phys*, vol. 121, no. 3, pp. 465–471, Jun. 2010, doi: 10.1016/j.matchemphys.2010.02.009.

[62] L. J. Xu, Y. Y. Chen, Z. G. Liu, and F. T. Kong, "The microstructure and properties of Ti-Mo-Nb alloys for biomedical application," *J Alloys Compd*, vol. 453, no. 1–2, pp. 320–324, Apr. 2008, doi: 10.1016/j.jallcom.2006.11.144.

8   APPENDICES

Appendice 1. β-Type Titanium alloys systems classification[10]

(a) Binary system	(b) Ternary systems	(c) Quaternary systems
Ti-Nb system	Ti-Nb-Mo system	Ti-Ta-Sn-Zr system
Ti-Mo system	Ti-Nb-Pd system	Ti-Nb-Zr-Sn system
Ti-Ta system	Ti-Nb-Zr system	Ti-Nb-Zr-Fe system
Ti-Zr system	Ti-Nb-Sn system	Ti-Nb-Ta-Zr system
Ti-Mn system	Ti-Nb-Ta system	Ti- Mo-Zr-Fe system
Ti–Cr system	Ti-Nb-Fe	Ti-Fe-Ta-Zr system
	Ti-Mo-Zr system	Ti-Cr-Mn-Sn system
	Ti-Mo-Nb system	
	Ti-Cr-Al system	
	Ti–Cr–Nb system	
	Ti-Cr-Sn system	
	Ti–Mn–Al	
	Ti-Ta-Nb system	
	Ti-Ta-Sn system	
	Ti-Ta-Zr system	
	Ti–Mn–Fe	
	Ti–Sn–Cr	

Appendice 2. Literature review β-Titanium Alloys with Reduced Young's Modulus

Ref	Alloy composition	Young Modulus (GPa)	Conclusions
[12]	Ti-23Nb-7Zr	35.99	*Ti-23Nb-7Zr has the highest hardness and Young's modulus values. *Nb content significantly influenced Young's modulus and hardness properties of Ti-xNb-7Zr alloys. *Ti-33Nb-7Zr exhibited reduced hardness and Young's modulus, with the β-phase covering most of the surface.
	Ti-28Nb-7Zr	29.1	
	Ti-33Nb-7Zr	29	
[46]	Ti-29Nb-13Ta-2Sn	45	*The tensile strength and elongation of the Ti–29Nb–13Ta–4.6Zr alloy are either equivalent to or exceed those of conventional titanium alloys commonly utilized in implant applications. *The Young's moduli of the newly designed alloys are significantly lower compared to Ti–6Al–4V ELI *The beta-type titanium alloys developed in this research, such as Ti–Nb–Ta–Zr, Ti–Nb–Ta–Mo, and Ti–Nb–Ta–Sn system alloys, are anticipated to offer superior performance as implant materials.
[24]	Ti-11Nb-7Fe	86	*Nb addition enhances stability and proportion of β phase in alloys. *Ti-11Nb-7Fe alloy exhibits lower elastic modulus and higher compressive strain. *The wear resistance of Ti-xNb-7Fe alloys is reduced by increasing their Nb content.
[47]	Ti–25Nb–3Fe	65	*Phase transformations in Ti-Nb-Fe alloys influence elastic modulus. *Anelastic relaxation spectra provide detailed kinetics of phase transformations. *Nb content stabilizes β-phase, influences ω-phase precipitation temperatures. *Ti-25Nb-3Fe alloy shows the lowest elastic modulus of 65 GPa.
[48]	Ti–35Nb–7Zr–6Ta–2Fe–0.5Si	85	*Fe and Si improved mechanical properties and biocompatibility of TNZT alloy. *TNZT-2Fe-0.5Si alloy is a promising candidate for load-bearing implants.
[49]	Ti–7Fe–11Nb	84	*Nb enhances β phase stability, reducing α'' phase formation during quenching. *Ti-7Fe-11Nb alloy has single β phase microstructure, high deformability. *Ti-7Fe-11Nb shows lowest Young's modulus, highest plastic deformation.
[50]	Ti–24Nb–4Zr–8Sn	56	*Warm swaging and rolling refine grains, enhancing Ti alloy properties. *Warm rolling increases tensile strength significantly while retaining good ductility
[51]	Ti-27Nb-7Fe-8Cr	72	*Single β phase in Cr-containing alloys, two-phase in Ti-27Nb-7Fe. *All alloys show high compressive strength and plastic strain. *Ti-27Nb-7Fe suitable for high strength applications, Ti-27Nb-7Fe-8Cr for low modulus.
[52]	Ti-5.4Nb	35	*Ti-Nb alloys showed biocompatibility without toxic effects. *Proper porosity in implants enhances biocompatibility with bone tissue. *Successful integration between implant and bone tissue requires proper porosity.
[53]	Ti–6Al–3Fe	97	*Fe addition enhances compressive strength and reduces fine pores. *Ti-6Al-3Fe shows the highest strength/modulus ratio for biomedical applications. *Excessive Fe leads to large pores, limiting sintering response benefits.
[54]	Ti–19Zr–10Nb–1Fe	59	*Ti-19Zr-10Nb-1Fe alloy has good superelasticity, corrosion resistance, and biocompatibility. *Fe1.0 alloy shows low corrosion rate and high mechanical properties. *As-quenched Fe1.0 alloy has better hemocompatibility than NiTi alloy.
[42]	Ti–5Zr	80	*Ti-Zr alloys showed α' phase formation with increased microhardness. *Elasticity modulus varied with zirconium concentrations but remained within range. *Biocompatibility tests indicated no cytotoxic effects on osteoblastic cells.
[13]	Ti-15Mo-0.5Si	19.81	*New Ti-based alloys show improved properties for medical applications. *Ti alloys with stabilizing elements have modulus close to human bone. *New compositions with nontoxic elements like Mo, Si, Zr, and Ta
	Ti-20Mo-0.5Si	37.53	
	Ti-15Mo-7Zr-10Ta	76.88	
	Ti-20Mo-7Zr-10Ta	43.41	
[55]	Ti–15Zr–10Cr	78	*Ti-15Zr-3Cr and Ti-15Zr-10Cr are potential biomedical materials. *Ti-15Zr-xCr alloys exhibit high microhardness, yield strength, and ductility. *Cr addition influences phase constitutions and mechanical properties of Ti alloys. *Cr is a promising alloying element for Ti base alloys.
[11]	Ti–30Zr–6Mo	60	*Ti-30Zr-7Mo alloy is highly cytocompatible. *Ti-30Zr-(6, 7 wt.%)Mo alloys show low Young's modulus, high strength.

Appendice 3. Literature review β-Titanium Alloys with enhanced wear resistance

Ref	Weight percentage of elements (wt%)									Coments	Total compositon	Trend	Type system	Units
	Nb	Ta	Mo	Sn	Cu	Zr	Al	Fe	Ti					
[21]					12%					Ti-12Cu alloy compared to Ti-7.1Cu and Ti-3Cu and Comparison Ti-cp.	Ti-12Cu	Cu	binary	mm^3
[24]	4%							7%		A series of Ti-xNb-7Fe alloys with varying niobium (Nb) concentrations (x=0, 1, 4, 6, 9, 11 wt.%)	Ti-4Nb-7Fe	Nb	ternary	wear rate (m^3/m)
[24]	6%							7%			Ti-6Nb-7Fe	Nb	ternary	wear rate (m^3/m)
[25]	5%		15%							Ti−15Mo−xNb (x=5, 10, 15 and 20).	Ti−15Mo−5Nb	Nb	ternary	friction coefficient
[9]	5.3%	31%				41.7%			21.90%	Ti45-Zr45-Nb5-Ta5, Ti42.5-Zr42.5-Nb5-Ta10, Ti40-Zr40-Nb5-Ta15 and comparison Ti-6AL-4V.	Ti40-Zr40-Nb5-Ta15 (E=59.3±2.1 Gpa) *at%	Ta	quaternary	wear rate (mm^3/Nm)
[26]	3.5%						6%			The Ti−based alloys in the composition of Ti−6Al−xNb (x = 3.5, 7,10.5, 14, 17.5, and 21 wt%).	Ti−6Al−3.5Nb	Nb	ternary	wear rate (mm^3/Nm)
[27]	5%				5%					Ti−5Cu-(x%) Nb (x = 0, 5, 10, and 15 wt%).	Ti−5Cu−5Nb	Nb	ternary	Wear rate (mm^3/mm) volumetric wear ×10^{-3} (mm^3)
[28]	5%									binary Ti-Nb alloys for dental prostheses with niobium contents ranging from 5% to 20% were investigated(5,10,15,20).	Ti-5Nb	Nb	binary	wear scar depth
[39]	30%			2%						Ti-30Nb, Ti-30Nb-2Sn, Ti-30Nb-4Sn. Wt%.	Ti-30Nb-2Sn	Sn	ternary	friction coefficient

Appendice 4. Literature review β-Titanium Alloys with higher hardness vickers

Ref	Weight percentage of elements (wt%)										Coments	Total compositon	Trend	Type system	units [ref=346 HV for Ti-6Al-4V]
	Nb	Ta	Mo	Sn	Zr	Fe	Si	Ti	Mn	Cr					
[33]			12.5%								Ti-xMo (6 to 20 wt%).	Ti-12.5Mo	Mo	binary	340 HV
[47]	10%					3%					Beta Ti–xNb–3Fe (X=10, 15,20 and 25wt%)	Ti-10Nb-3Fe	Nb	ternary	479 HV
[49]	4%					7%					A series of Ti–7Fe–xNb (x=0, 1, 4, 6, 9, 11 wt.%)	Ti–7Fe–4Nb	Nb	ternary	(325–520 Hv)
[49]	6%					7%						Ti–7Fe–6Nb	Nb	ternary	
[13]			15%				0.50%				Ti-15Mo-0.5Si, Ti-20Mo-0.5Si, Ti-15Mo-7Zr-10Ta, Ti-20Mo-7Zr-10Ta	Ti-15Mo-0.5Si	Mo	ternary	233.37 HV
[13]		10%	15%		7%							Ti-15Mo-7Zr-10Ta	Mo	ternary	462.33 HV
[56]	25%					7%					Ti-25Nb-xFe (0,1,3,5,7 wt%).	Ti-25Nb-7Fe	Fe	ternary	350.7 HV
[55]					15%					5%	Ti–15Zr–xCr (0 ≤ x ≤ 10, wt.%).	Ti-15Zr-5Cr	Cr	ternary	(307–519 HV)
[57]	35%			2.50%							Ti–35Nb-XSn alloys (x = 2.5; 5; 7.5 wt%)	Ti-35Nb-2.5Sn	Sn	binary	>300 HV
[58]	24%				4%				5%		A series of Ti-24Nb-4Zr-xMn (x = 0, 1, 3, and 5 wt%).	Ti-24Nb-4Zr-xMn	Mn	quaternary	429 HV
[59]					6%	7%					A series of ternary Ti-6Zr-xFe (x = 4, 5, 6, 7 wt %) .	Ti-6Zr-7Fe	Fe	ternary	348 HV
[60]		15%	15%		7%		1%				Ti-15Mo-7Zr-15Ta, Ti-15Mo-7Zr-15Ta-0.5Si, Ti-15Mo-7Zr-15Ta-0.75Si, Ti-15Mo-7Zr-15Ta-1Si.	Ti-15Mo-7Zr-15Ta-1Si.	Si		362.83 HV
[61]					10%					5%	Ti–10Zr–xCr alloys with 1, 3, 5, 7 and 10 wt.% Cr.	Ti-10Zr-5Cr	Cr	ternary	384 HV

[35]			15%	10%			2%	Ti-15Mo-6Zr-xCr (x = 1, 2, 3, 4 wt.%).	Ti-15Mo-6Zr 2Cr	Cr	quaternary	412 HV
[62]	3%		10%					Ti–10Mo–nNb alloys (n = 3, 7, 10)	Ti–10Mo–3Nb	Nb	ternary	441 HV
[30]	15.53%	30.24%		35.57%		18.66%		Ti 35 Zr 35 Nb 15 Ta 15 , Ti 30 Zr 30 Nb 20 Ta 20 , Ti 25 Zr 25 Nb 25 Ta 25 , and Ti 20 Zr 20 Nb 30 Ta 30 (at%)	Ti 35-Zr 35-Nb 15 -Ta 15		quaternary	642 HV
[30]	19.26%	37.5%		28.36%		14.88%			Ti 30- Zr 30- Nb 20- Ta 20		quaternary	583 HV
[30]	22.50%	43.82%		22.09%		11.59%			Ti 25 -Zr 25- Nb 25- Ta 25		quaternary	541 HV
[30]	25.30%	49.4%		16.59%		8.70%			Ti 20 -Zr 20- Nb 30- Ta 30		quaternary	519 HV

Appendice 5. preparation method for titanium alloys

Struers
Ensuring Certainty

Titanium Alloys   1417

Grinding

Steps		PG	FG
Surface	**Type**	MD-Mezzo 220	MD-Largo
	Disc speed (rpm)	300	150
Abrasive	**Type**		DiaPro Allegro/Largo 9 µm
	Predosing/dosing		3/6
Lubricant	**Type**	Water	
	Predosing/dosing		
	Force (N)	40	30
	Holder direction	>>	>>
	Holder speed (rpm)	150	150
	Time (min)	1	4

Polishing

Steps		OP
Surface	**Type**	MD-Chem
	Disc speed (rpm)	150
Abrasive	**Type**	OP-S, 0.25 µm
	Predosing/dosing	1/10
Lubricant	**Type**	
	Predosing/dosing	
	Force (N)	30
	Holder direction	><
	Holder speed (rpm)	150
	Time (min)	5

Method comments

The method is developed to fit a standard equipment configuration with 30 mm specimen on 300mm disc. Dosing levels are valid for following equipment: Tegramin, AbraPol and LaboPol

For advice on how to adjust the method to fit your equipment, please take a look at Preparation Parameters.

The preparation time for the plane grinding (PG) step depends very much on the condition of the samples and if they are prepared as single specimens or clamped in a specimen holder. Please check the samples after the first step and repeat it if necessary.

Take a look at Preparation Parameters ⊙

Appendice 6. EDS spectrum of Ti-Zr-Nb-Ta alloys a)Ti-40Zr-4Nb-33Ta b)Ti-30Zr-4Nb-33Ta c)Ti-20Zr-4Nb-33Ta

a) Ti-30Zr-4Nb-10Mo
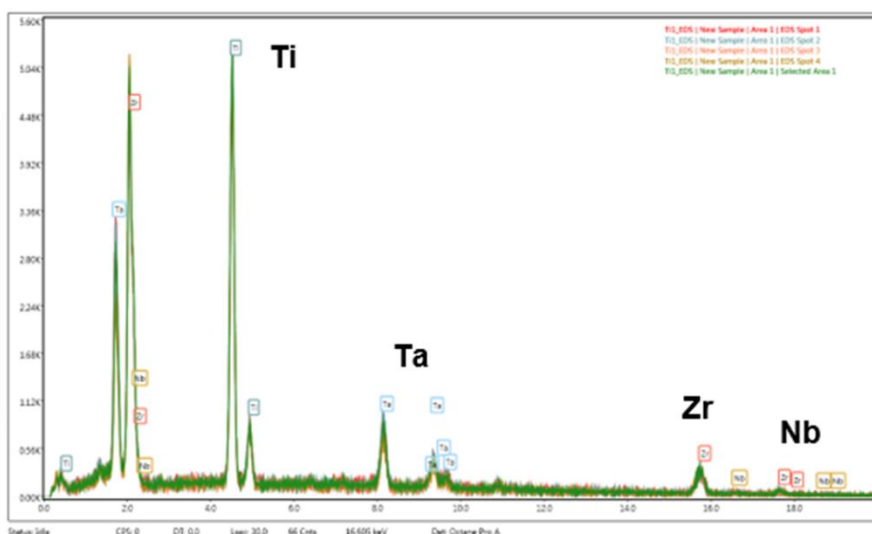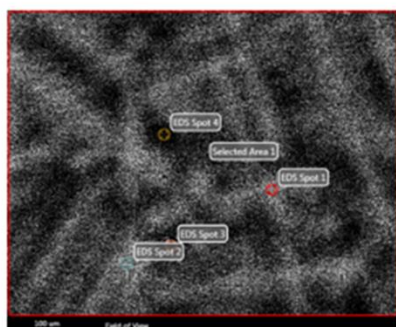
b) Ti-30Zr-4Nb-13Mo

c) Ti-30Zr-4Nb-16Mo

d) Ti-6Al-4V

Appendice 8. Nanoindentation results

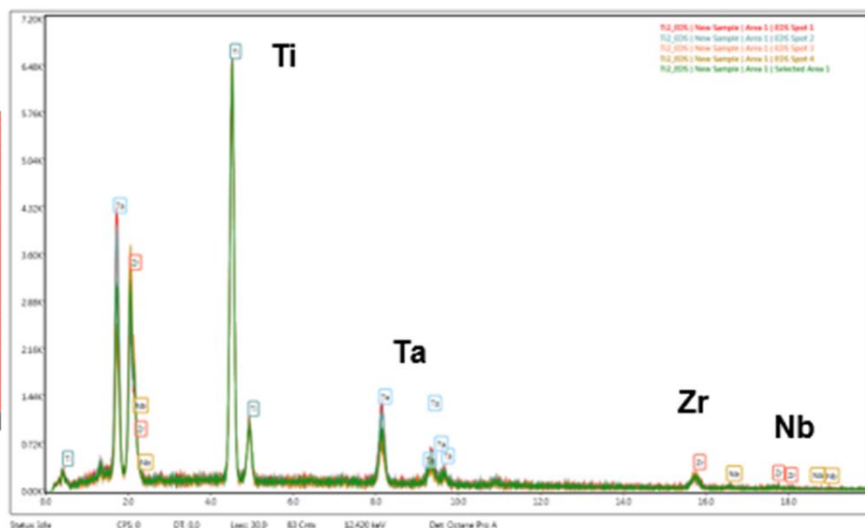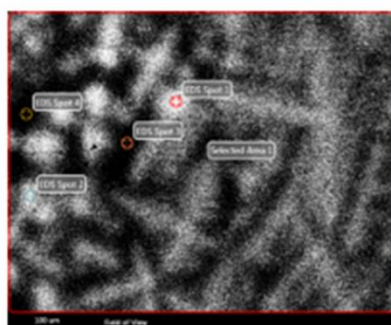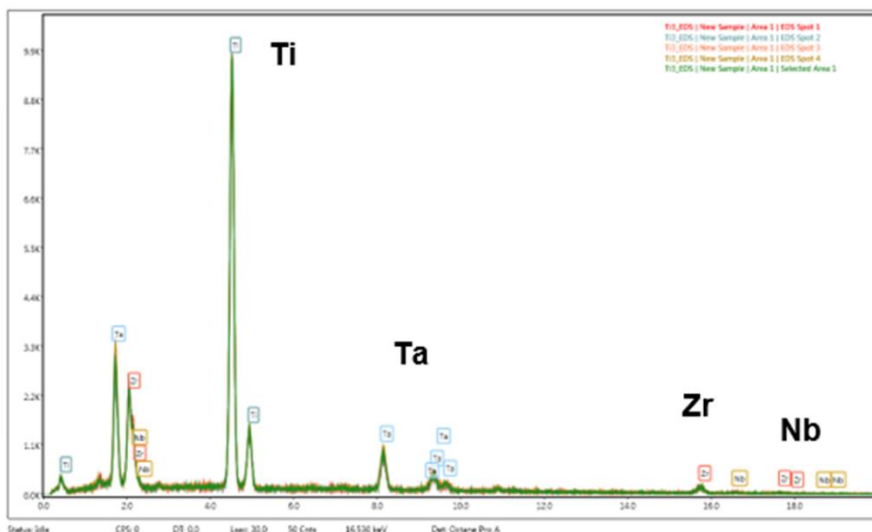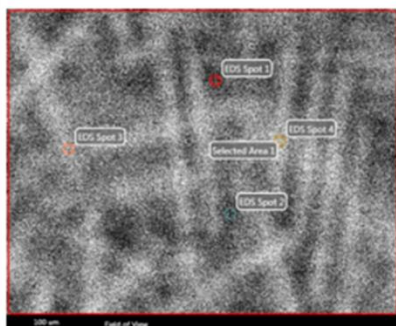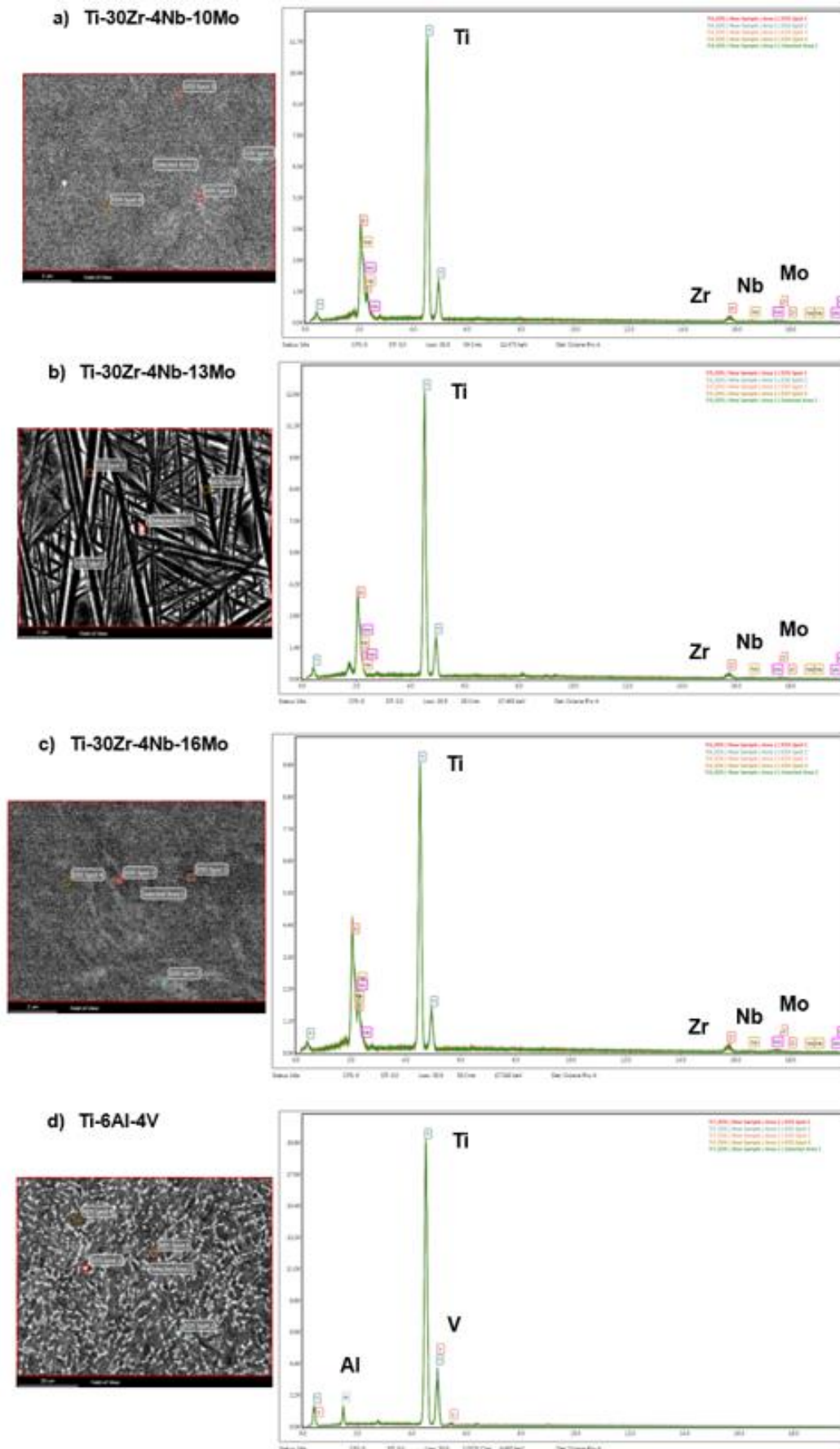| Indent	Ti-40Zr-4Nb-33Ta		Ti-30Zr-4Nb-33Ta		Ti-20Zr-4Nb-33Ta		Ti-30Zr-4Nb-10Mo		Ti-30Zr-4Nb-13Mo		Ti-30Zr-4Nb-16Mo		Ti-6Al-4V
	H (Gpa)	E (Gpa)	H (Gpa)	E (Gpa)	H (Gpa)	E (Gpa)	H (Gpa)	E (Gpa)	H (Gpa)	E (Gpa)	H (Gpa)	E (Gpa)	E (Gpa)
1	omitted	omitted	omitted	omitted	4.38	90	omitted	omitted	omitted	omitted	4.89	107	118
2	4.20	97	3.92	80.48	4.50	90	4.15	68	omitted	omitted	5.04	107	118
3	4.26	97	3.97	79.43	4.42	88	omitted	omitted	omitted	omitted	5.01	109	122
4	4.19	96	4.10	79.81	4.34	87	4.23	67	omitted	omitted	5.27	110	122
5	omitted	omitted	4.18	79.80	4.40	89	omitted	omitted	omitted	omitted	5.40	106	118
6	4.47	98	4.29	79.97	4.44	88	4.41	69	3.63	69	5.50	106	123
7	4.44	97	4.18	78.81	4.51	88	4.31	68	3.76	71	5.48	108	122
8	omitted	omitted	4.16	79.21	4.38	87	4.36	69	3.84	72	5.31	107	120
9	4.34	94	4.09	80.40	4.50	89	4.25	68	3.82	72	5.20	108	118
10	4.35	97	omitted	omitted	4.56	89	omitted	omitted	3.88	71	5.75	107	121
11	4.46	98	4.45	86.56	4.51	89	4.44	71	4.03	73	5.52	110	121
12	4.45	98	4.29	85.68	4.47	88	4.64	74	3.95	74	5.46	110	118
13	4.35	95	4.33	86.93	4.54	89	4.49	71	4.00	75	5.26	112	126
14	4.36	98	4.50	86.59	4.43	89	4.53	73	4.05	75	omitted	omitted	120
15	4.41	97	omitted	omitted	4.51	89	omitted	omitted	4.00	74	omitted	omitted	omitted
16	4.38	98	4.34	86.95	4.53	90	4.59	74	4.15	76	omitted	omitted	119
Average	4.4	97	4.2	82	4.5	89	4.4	70	3.9	73	5.3	108	120
Standard deviation	0.09	1.13	0.17	3.49	0.07	0.89	0.16	2.50	0.15	2.10	0.24	1.77	2.32

Appendice 9. hardness vickers measurements

Indent	Ti-40Zr-4Nb-33Ta	Ti-30Zr-4Nb-33Ta	Ti-20Zr-4Nb-33Ta	Ti-30Zr-4Nb-10Mo	Ti-30Zr-4Nb-13Mo	Ti-30Zr-4Nb-16Mo	Ti-6Al-4V
1	268	282	302	330	334	264	299
2	269	279	290	319	338	266	297
3	270	293	281	316	323	268	302
4	267	285	282	325	321	267	301
5	268	292	283	331	319	268	300
6	273	283	280	338	332	270	300
7	264	280	298	331	345	271	297
8	270	287	300	331	346	270	300
Average	269	285	290	328	332	268	300
Standard deviation	2.62	5.22	9.26	7.21	10.53	2.33	1.77

Appendice 10. Electrochemical parameters determined from the OCP curves for Ti-Zr-Nb-Ta alloys vs Ti-6Al-4V

	Ti-40Zr-4Nb-33Ta			Ti-30Zr-4Nb-33Ta			Ti-20Zr-4Nb-33Ta			Ti-6Al-4V		
	6 N	17.5 N	30.8 N	6 N	17.5 N	30.8 N	6 N	17.5 N	30.8 N	6 N	17.5 N	30.8 N
E_{OCP} (mV vs Ag|AgCl)	-463.15	-286.89	-353.24	-306.86	-288.68	-493.13	-332.45	-296.95	-357.28	-182.88	-111.84	-234.26
Standard deviation EOCP	19	3	8	1	10	11	17	2	9	9	2	22
E_{wear} (mV vs Ag|AgCl)	-688.06	-674.28	-744.12	-604.73	-774.50	-860.83	-721.04	-815.17	-666.55	-678.09	-769.87	-786.77
Standard deviation Ewear	34	22	17	15	15	35	58	29	106	72	62	62
$|\Delta E|$ (mV vs Ag|AgCl)	224.91	387.39	390.88	297.87	485.82	367.69	388.58	518.22	309.27	495.21	658.03	552.51

Appendice 11. Electrochemical parameters determined from the OCP curves for Ti-Zr-Nb-Mo alloys vs Ti-6Al-4V

	Ti-30Zr-4Nb-10Mo			Ti-30Zr-4Nb-13Mo			Ti-30Zr-4Nb-16Mo			Ti-6Al-4V		
	6 N	17.5 N	30.8 N	6 N	17.5 N	30.8 N	6 N	17.5 N	30.8 N	6 N	17.5 N	30.8 N
E_{OCP} (mV vs Ag|AgCl)	-309.67	-273.49	-246.27	-324.52	-260.43	-295.35	-322.55	-296.89	-293.50	-182.88	-111.84	-234.26
Standard deviation EOCP	4	8	14	17	2	7	2	28	8	9	2	22
E_{wear} (mV vs Ag|AgCl)	-614.22	-705.73	-740.05	-777.79	-757.86	-844.36	-649.94	-642.31	-709.07	-678.09	-769.87	-786.77
Standard deviation Ewear	54	38	24	62	26	31	53	33	42	72	62	62
$|\Delta E|$ (mV vs Ag|AgCl)	304.56	432.23	493.78	453.27	497.43	549.01	327.39	345.42	415.57	495.21	658.03	552.51

Appendice 12. Equations Oliver and Pharr method

Generally, hardness (H) is defined as the ratio of the maximum applied load (P_{Max}) to the projected area of the indentation (A), as described by the following equations[37]

$$H = \frac{P_{Max}}{A}$$

(1)

The contact stiffness, S, was determined from the initial slope of the unloading curve as follows:

$$S = \frac{dP}{dh}$$

(2)

P is define as the applied load h and is define as the penetration depth during the test. The elastic modulus was subsequently calculated based on its relationship with the contact area (A) and the contact stiffness:

$$S = \beta \frac{2}{\sqrt{\pi}} E_r \sqrt{A}|$$

(3)

The term β is a constant dependent on the indenter's geometry and is equal to 1.034 for a Berkovich indenter[38]. E_r is the reduced elastic modulus, which accounts for the elastic contributions of both the specimen and the indenter tip, defined as follows:

$$\frac{1}{E_r} = \frac{1 - v^2}{E} + \frac{1 - v_i^2}{E_i}$$

(4)

here, E_i and E are the respective elastic modulus of the indenter and sample, whereas v_i and v are the Poisson's ratio of the indenter and the specimen respectively.